Circulation Control Technique on a Marine Propeller Duct

Craig Christopher Ward

Department of Naval Architecture & Marine Engineering
Universities of Glasgow and Strathclyde
Henry Dyer building
100 Montrose Street
Glasgow
U.K.
G4 0LZ

Thesis submitted to the
University of Strathclyde
for the degree of
Master of Science in Marine Engineering

August 2006

Copyright Notice

Abstract

A modified marine propeller duct that implements the circulation control technique is presented. The modification allows the conventional control planes to be removed from a marine vehicle such as an AUV whilst maintaining a suitable manoeuvring force. It is shown that for an AUV, a manoeuvring force improvement of over 600 % at 1 Knot is possible. The manoeuvring force at higher speed is at least equal to the original control surfaces. Efficiency is shown to be increased by 9.5 % for the same manoeuvring force. A non-ducted circulation control propeller is also proposed.

Acknowledgements

Thanks to my supervisor, Dr Phil G. Sayer for his help.

Contents

List of Tables

List of Figures

Chapter 1. Introduction

Increasingly, more interest is being shown into using Autonomous Underwater Vehicles (AUVs) in the military, ocean research and commercial marine sectors. Figures 1.1 and 1.2 picture two typical vehicles. Typically, AUVs are designed to be programmed with a mission and then launched from a ship. They then follow a predefined route whilst collecting data e.g. scanning the ocean bed using sonar. When the mission is complete, the vehicle meets with the support ship where it is recovered (Griffiths, 2001). One of the major practical problems currently encountered when using AUVs is the difficulty of launch and recovery (Bingham, 2002). During this time, the AUV is most likely to be damaged due to a collision or impact during handling. It is therefore important that an AUV should be as robust as possible (Subsea7, 2003).

Figure 1.1. U.S. Navy Seahorse AUV (ONR, 2006).

Figure 1.2. Geosub AUV (Subsea7, 2003).

Most systems of the AUV are situated inside the hull and are therefore protected. The propeller and the control surfaces that manoeuvre the vehicle are situated outside and at the extremities of the vehicle, therefore they are most likely to be damaged.

The new concept proposed in this report is essentially a modified propeller duct that can produce a manoeuvring force by redirecting the main propeller thrust using a technique called circulation control. This uses secondary high-velocity water jets and the Coanda effect at the trailing edge to alter the pressure distribution around the duct. This causes the propeller thrust to be deflected. Figure 1.3 shows the section and the expected flow around the modified duct. This allows the traditional control surfaces to be removed and all the moving parts associated with the new system (primarily a water pump) can be situated inside the hull. This should result in increased reliability and reduced vulnerability to external damage.

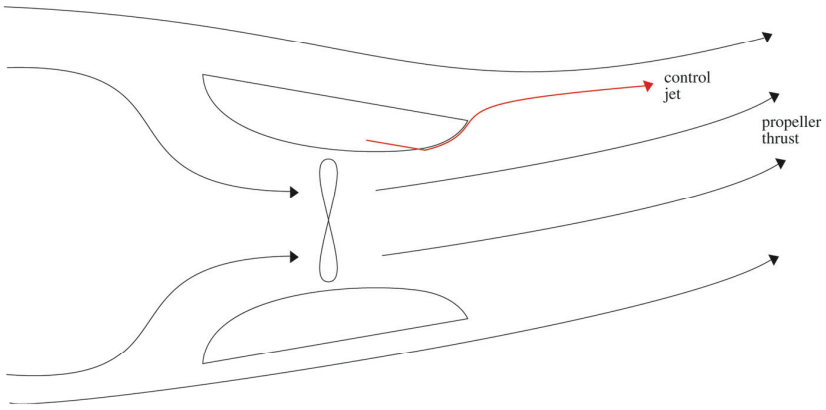

Figure 1.3. Cross section view of modified duct showing effects on flow when circulation control is activated on starboard side of the duct.

Circulation control is an active technique that alters the pressure distribution around a hydrofoil or airfoil and as a result, the lift force can be dramatically improved (Rogers 2004). Figure 1.4 shows a typical circulation control system implemented at the trailing edge of an airfoil (Englar, 2004a). Circulation control is normally researched for its aeronautical applications since its vertical lift augmentation properties make it attractive for short take off and landing aircraft (STOL) (Englar,

2004b). The proposed marine system takes advantage of this same technique and applies it to a propeller duct. A non-ducted propeller design is also proposed in the future work section.

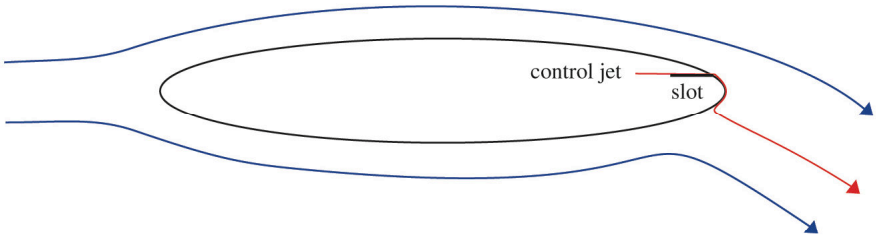

Figure 1.4. Circulation control airfoil.

Ducted propellers are normally used in applications where there is a high thrust coefficient (Breslin, 1994). This includes some AUVs, tugboats, trawlers and some large bulk carriers and tankers etc. Figure 1.1 shows a duct fitted to an AUV and figure 1.5 shows a typical ducted propeller installation on a small ship. Most modern tugboats use azimuthing ducted propellers and it is difficult for any manoeuvring system to compete with the thrust vectoring capability of these devices. Therefore, the application of the proposed circulation controlled duct would be best aimed at AUVs, trawlers, tankers, bulk carriers, high performance naval applications and other marine vehicles using fixed ducts.

Figure 1.5. Rear view of a Kort nozzle (ducted propeller) with single rudder. (Olds, 2006)

Chapter 2. Aims of the project

The overall aim of the project was to show that the circulation control technique could be used on an AUV using a ducted propeller to generate a manoeuvring force at a efficiency that is at least equal to the traditional control surfaces. Using circulation control on the propeller duct allows the removal of the traditional control surfaces.

To prove the merits of the new system, analysis was required in the following areas,

1. Comparison of the manoeuvring force (induced lift force) of the new circulation control duct system against a traditional AUV control surface system.

2. Specification of major profile changes and structural changes required to be made to the original duct.

3. Efficiency comparison of the new circulation control duct system against a traditional AUV control surface system.

Chapter 3. Critical Review

3.1 Critical review

The main papers of interest to this project can be considered to belong to one of three areas. These are,

1. Circulation control papers, aeronautical related.
2. Circulation control papers, marine related.
3. Propeller duct related papers.

The papers investigating circulation control in the aeronautical and marine sectors are very closely related. One of the main differences is that the marine applications of circulation control are typically implemented on control surfaces that have a lower aspect ratio when compared to an aircraft wing (Rogers, 2006).

Circulation control is dependent on the Coanda effect. This effect is the ability of a flow of air or fluid to adhere to a curved surface causing a deflection. A simple example is holding the back of a spoon under a running tap of water. The Coanda effect is named after Henri Coanda, a famous Romanian aviation pioneer who observed the effect. He first noticed the effect in about 1910 after attaching a curved steel plate to protect his wooden plane from hot engine exhaust gasses. Instead of protecting the plane, the curved plate caused the gasses to be redirected onto the fuselage causing the plane to catch fire (Wood, 1986).

It is useful to define the momentum coefficient early in this report. This describes the relative momentum of the high speed control jet. Assuming 2D incompressible flow, it can be described by any of the following equivalent equations.

$$C = \frac{\dot{m}_j \cdot V_j}{q \cdot A} \qquad C = \frac{\dot{m}_j \cdot V_j}{\frac{1}{2} \cdot \rho \cdot V_{inf}^{2} \cdot A} \qquad C = 2 \cdot \frac{h}{c} \cdot \left(\frac{V_j}{V_{inf.}} \right)^2$$

mr_j = Mass flow rate of jet	V_{inf} = Velocity of freestream
V_j = Velocity of jet	ρ = Density of main flow
q = Dynamic pressure	A = Wing planform area
h = Slot height	c = Wing chord length

Modern circulation control research is aimed at augmenting lift of aircraft wings and marine control surface although the vast majority of research has been done in the aviation field. Initial papers were presented by Kind (1967) and Cheeseman (1967) showing that such a jet blowing system can produce lift coefficients in excess of 2 for an elliptical symmetrical airfoil at zero angle of attack. This is clearly impressive given that the wing only requires modification at the trailing edge.

The initial research was done in the UK but interest declined after the 1960s, however, circulation control research activity increased in the USA. Of notable mention is the author Robert Englar. He has published many papers on the subject over several decades e.g. Englar (1971) and Englar (2004a). He also produced an excellent bibliography that details work carried out over the period 1967 to 1983 (Englar, 1983). It is clear that Englar is more enthusiastic about the technology rather than the application and is currently working on using the technology to reduce drag on large road vehicles (Englar, 2004a).

It is this author's view that circulation control is still very much a solution looking for a problem and that the complete system performance gain of circulation control is not sufficient to justify its use in aircraft for vertical lift augmentation. After 40 years of research, several flight demonstrators and large amounts of money, no current aircraft uses the technology to augment vertical lift. It is used for certain niche aeronautical applications and these are described in the next paragraph. Other authors also doubt its application for vertical lift applications citing it as a high-risk technology e.g. Bushnell, (2004) and Loth (2004). Bushnell states that the technology is still high risk since the research has not been taken far enough.

However given that Englar's (1983) bibliography cited 160 reports and papers this would suggest otherwise. Some researchers currently work on CFD of circulation control surfaces (e.g. Baker, 2004). However, if the fundamental technology does not offer sufficient overall advantages in vertical lift aeronautic applications to become adopted there seems little point in optimisation at the present time.

Two aircraft are currently known to use a circulation control although not primarily for its high vertical lift properties. The commercially successfully No Tail Rotor Helicopter (NOTAR) uses circulation control to replace the tail rotor on a helicopter. This is shown in figure 3.1. The circulation control acts along the length of the tail to divert the main rotor's thrust to create a horizontal force component. This removes the need for a tail rotor. However, the system still requires a jet thruster at the end of the tail to allow sufficient manoeuvring control.

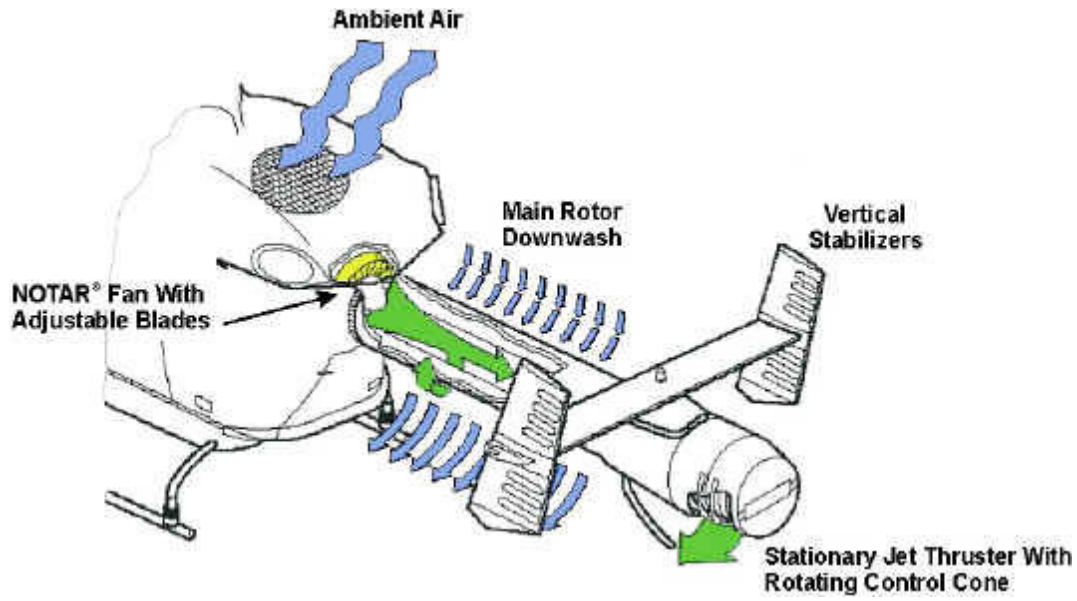

Figure 3.1. NOTAR helicopter. (MD helicopters, 2006).

Another aircraft to use circulation control is the vertical take off and landing (VTOL) Bell Boeing V-22 Osprey (Joslin, 2004). The aircraft is pictured in figure 3.2. Ironically (given Coanda's original fiery exploits) it uses circulation control to

deflect hot exhaust gasses away from the fuselage when the aircraft is on the ground to protect certain avionic systems. Circulation control was deemed the most cost effective way of achieving this.

Although both these aircraft successfully use circulation control they are niche applications and do not take advantage of circulation control's impressive potential for vertical lift augmentation.

Figure 3.2. Bell Boeing V-22 Osprey (airforce-technology, 2006)

Most of the research into circulation control in hydrodynamics has been done into its implementation at the trailing edge of a control surface or rudder to augment lift of the device. Papers have been published regarding the testing of such hydrodynamic devices in wind tunnels and water channels and these are discussed in the following pages. It is unlikely that any such device has been implemented on a test vehicle etc. Joslin (2004) says that this would be the next logical development step.

Englar at the Naval Ship Research and Development Centre in the U.S. was involved in the design and model testing of non-moving submarine stern planes using circulation control to generate lift (Englar, 1971). The planes were the same size as normal stern planes, and with moderate blowing the manoeuvring requirements of the submarine were met or exceeded. The report also evaluated the performance of end plates. This report is very useful and addresses the question of Coanda diameter limits and slot height limits. It also details a method of comparing efficiency with

the conventional appendage. Although useful and used in this thesis, this method of comparing efficiency between the two systems has limitations. It does not explicitly emphasise the fact that to maintain a constant lift force, the circulation control system will always incur a running cost and fuel penalty while the rudder, once moved, does not require any extra power. This is a problem associated with comparing a passive system with an active system. For this reason, the power required to produce the water jet has also been calculated independently in this thesis.

A high lift rudder was investigated by Zhu (1996) at Wuhan University in China. This showed useful lift augmentation effects using a modified NACA 0015 (symmetrical) airfoil with a blown slot at a round trailing edge. This is shown in figure 3.3. Zhu also investigated the use of endplates to reduce tip vortexes and the effects of grooves to decrease drag caused by the round bluff trailing edge. The work is useful in that it proposes the use of circulation control on a ship's rudder and uses a well known NACA airfoil. It also confirms high lift capability for marine applications. Zhu references other well known aeronautical papers in the circulation control field but he does not reference the 1971 marine application report by Englar. Englar's investigation was far more comprehensive and similarly considered endplates.

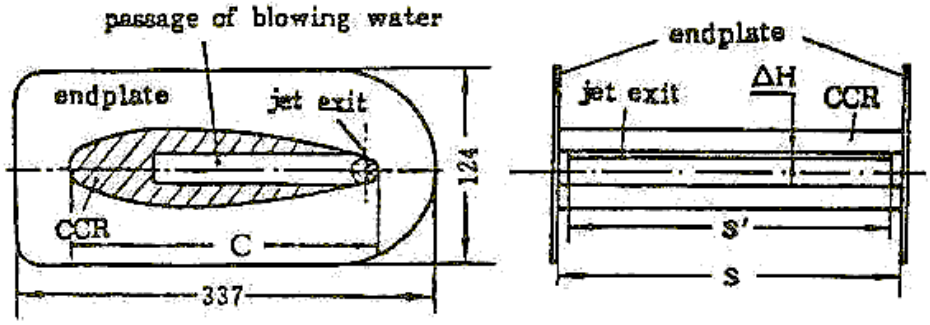

Figure 3.3. Single slot circulation control rudder based on NACA 0015. (Zhu, 1996).

Rogers (2004) investigated a low aspect ratio hydrofoil with dual blowing. i.e. upper and lower slots (figure 3.4). His report is comprehensive and also proposes that at higher jet momentum rates (≥0.3) the circulation controlled airfoil acts more like another type of lift augmentation system known as a jet flap and this causes lift generation to be less efficient. Generally, other authors have been at pains to distance the circulation control technique from the relatively inefficient jet flap e.g. Englar (2004a). Rodger's claims appear to be valid however, as the lift (C_L) versus control jet momentum (C_μ) curve is described by a square root term and at higher jet momentum the gradient is reduced and therefore the gains are lower.

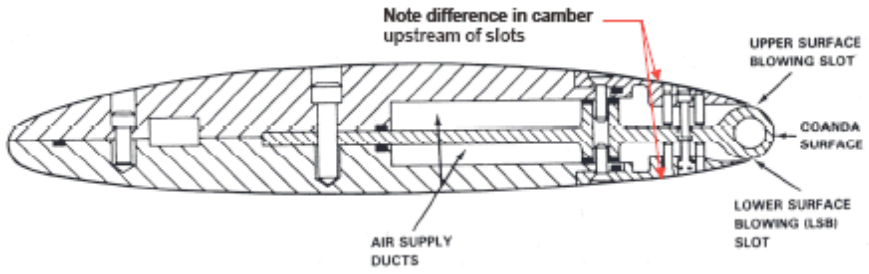

Figure 3.4 Low aspect ratio, dual slotted circulation control wing. (Rogers, 2004).

Rhee (2002) of Fluent Inc. investigated a CFD analysis of a blown flap hydrofoil. This was done in conjunction with previous experimental results by Ahn (2000) at Seoul National University in Korea. Ahn used a hydrofoil based on a symmetrical NACA 0021 profile. The blowing occurred at the rounded (Coanda surface) flap joint (figure 3.5). The flap tapered at the trailing edge to the original sharp NACA 0021 profile.

This concept has a fundamental limitation in that to generate lift, the flap would have to be first moved to reveal the Coanda surface. Only then would the circulation control have maximum effect and increase lift. Ahn does not present results to demonstrate what happens when blowing is used with a zero or small flap angle but it would most likely result in inefficient lift augmentation since Coanda attachment would not occur. The delay in moving the flap to a position where good attachment occurred would also reduce time response performance.

Essentially this method is improving lift performance by adding complexity to the rudder. As a result, it would appear that reliability would be reduced, maintenance costs would be higher and the initial cost of the system also higher. The system does have an advantage in that it retains the sharp trailing edge of the wing. This is advantageous since the profile drag will be maintained at a level close to the original section shape. Profile drag is an important issue with circulation control systems since a rounded Coanda surface is normally required at the trailing edge. Flapped circulation control airfoils for aeronautical systems have been investigated in the past but have never caught on. Englar (2004a) describes several designs that have been developed in the past.

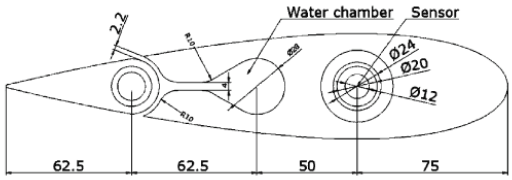

Figure 3.5. Blown flap Hydrofoil based on NACA 0021. (Ahn, 2000).

Joslin (2004) provides a useful high level overview of issues that face marine circulation control applications. Although it is simplistic, it is helpful, as most authors do not focus on the bigger picture. He poses some questions regarding performance degradation due to fouling, corrosion, noise, failure, cost and space requirements for a submarine circulation control stern plane system. Joslin does identify that there are "no apparent show stoppers" but that testing is required on a scaled platform. This is something that seems necessary since it would seem that there is currently enough data from testing of circulation control wings available in the literature to form the basis of a reasonable system. Howe (2002) mathematically investigated the effect of noise increases caused by circulation control on a hydrofoil. He identifies three sources of noise and states that if the Coanda jet is turbulent, its interaction with the slot lip dominates the high frequency noise. For a very thin slot lip thickness, the high frequency noise is typically 20dB greater than the noise from

the unmodified hydrofoil. Howe states that his own quantitative conclusions should be regarded tentatively since they are based on certain estimates. This thesis does not consider noise in detail but it is clearly an issue that would have to addressed.

A marine system very similar to the circulation control duct proposed by this project was investigated by Rogers in the 1990s. Limited information is available, but an overview of the work and key findings were presented by Imber (2004). The annular wing (or duct) tested had a symmetrical section and is shown in figure 3.6.

This appears useful, however, due to the way the duct was tested, the results are of limited use in this project. It appears that the main aim was to use the annular properties of the wing to increase lift performance. The annular shape results in a greater effective aspect ratio and combined with circulation control it is a high performance manoeuvring force producer. However, it does not appear that its use with a propeller was considered. The device was tested with similar flow rates on the inside and the outside of the duct. Clearly in most normal marine applications there is a propeller inside the duct and the flow is much faster on the inside.

In addition, the system was tested using two blown slits at the trailing edge of the duct (at the inner and outer edges). When a manoeuvring force was created using circulation control, the outer slot was blown at one side of the duct and the inner slit was blown at the other (complementary quadrants). However, if this method was used when the main flow was faster on the inside than the outside, the blowing from the outer slot would most likely decrease the manoeuvring force produced by the system.

One useful new finding of this investigation was the discovery that a braking force could be produced using alternating circulation control blowing. Alternating the active inside/outside slots every 90-degrees created two pairs of counter-rotating vortices. A drag coefficient of about 1 could be created for a blowing momentum of 0.1.

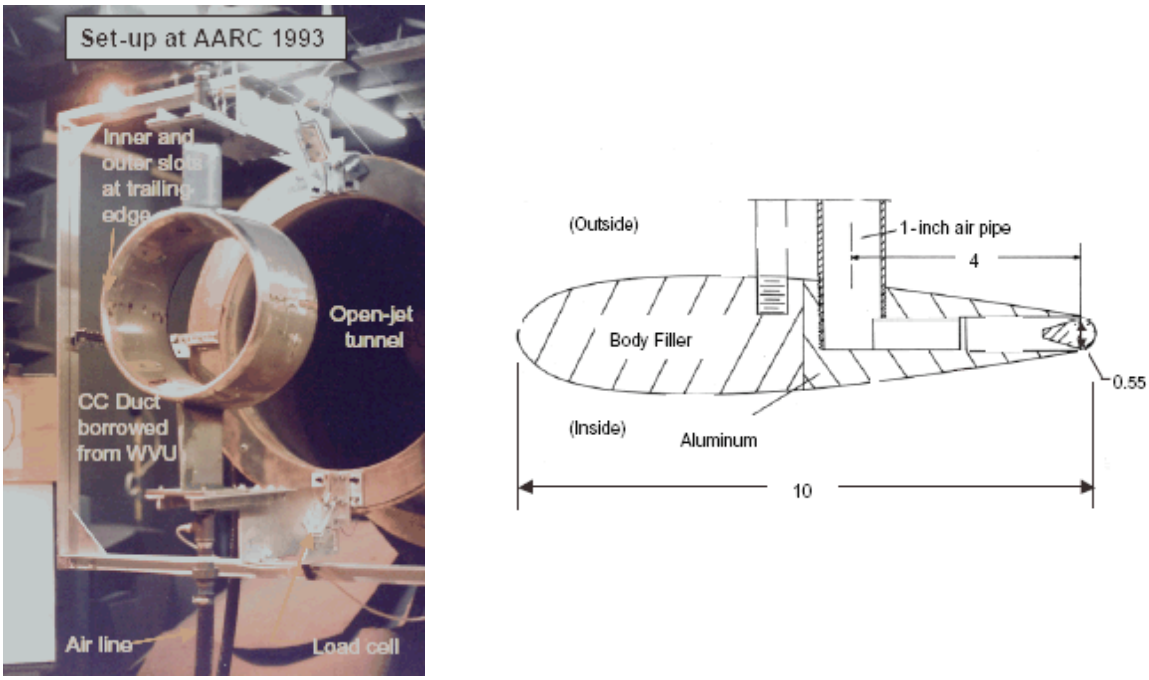

Figure 3.6. Circulation control annular wing / duct. (Imber, 2004).

Englar (2004b) tested a circulation control high lift wing that included a propeller mounted in a channel (figure 3.7). It can be seen that the wing channel configuration is similar in nature to the proposed marine circulation controlled duct. The real world use of this aircraft is perhaps questionable; Englar suggests one use would allow business aircraft to operate from shorter runways. However, the experimental results are useful and can be used to advantage in this project.

Figure 3.7. Super STOL aircraft. (Englar, 2004b).

Wind tunnel tests were carried out on a 0.075 semi-span scale model of the Super STOL aircraft. The effect of angle of attack, blowing momentum, propeller thrust and other variables on lift and drag were measured. Although many other papers test the basic properties of angle of attack and jet blowing momentum, the tests with the propeller thrust sets this paper apart. The flow in the propeller wake is complex so experimental results are important to predict the interaction between the wake and the circulation control blowing. The results are used extensively in the analysis section of this thesis so will be explained in detail there.

There is an interest at present to use circulation control for jet engine fluidic thrust vectoring particularly for Unmanned Air Vehicles (UAVs). Mason (2002) investigated the effect of changing the slot height and the Coanda diameter of a thrust vectoring circulation control rectangular nozzle (figure 3.8). This appears to be the first time a paper has been published with a series of tests like this. Other authors have simply chosen one fixed size of height and diameter. One issue with the tests is that they were done with a static external flow. This is not representative of normal operation and it is likely there will be some reduction in the lift forces that are achieved as the external flow increases in speed. It also complicates matters since the free stream has zero velocity and the Coanda blowing cannot therefore be described by the conventional momentum coefficient. However the results do show the relative effect of changing the parameters and Mason's Coanda diameter results have been used in the project's analysis.

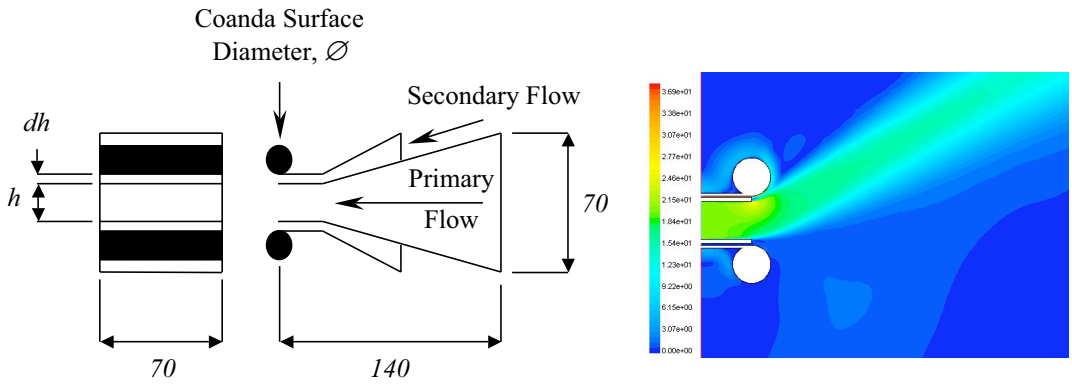

Figure 3.8. Jet engine fluidic thrust vectoring experimental setup and CFD visualisation. (Mason, 2002).

Propeller Ducts have been popular since the 1930's and accelerating ducts were experimentally proven to offer advantages in efficiency and thrust by Luisa Stipa and Ludwig Kort (Oosterveld, 1972). Decelerating nozzles are used in naval applications and are advantageous for reducing propeller cavitation. Much research has been done on ducted propellers and many of these papers are referenced by Sacks (1962) and Weissinger (1968)

The most common type of nozzle is the accelerating type and the most widely known sections are the MARIN 19a and 37. Oosterveld (1972) published the section shapes and provided extensive test data on these and other sections. His paper proposes the 19a as an approximation to aid manufacture of a slightly more streamlined section, the 19, which was also tested. However, this appears to be a strange jump in the paper and this point is also questioned by Mr C. Thew in the discussion after the 1973 Oosterveld paper. Mr Thew states that the 19a shape has been in widespread use in the U.K. and Germany since the early 1950s.

Generally, the work appears to be of a very high standard and also considers duct length whilst maintaining the section shape. Increasing the length is shown to slightly improve static bollard pull efficiency. No explanation is given for this increase in performance. As the length was increased, the duct section profile was maintained and therefore the lift force was also maintained, so lift would not have been the reason for the increase. The increase in force was most likely due to the increased separation of the nozzle exit and entrance. This effectively increased the re-circulation flow resistance outside of the duct from the exit to the entrance and would result in a greater thrust force being experienced by the duct.

Breslin (1989) covers ducted propellers and mathematically explains the circumstances in which they will result in an advantage. This reasonably high level analysis is useful as provides evidence of a duct's efficiency advantage. Unfortunately, he does not fully explain the fundamental operation of a duct. i.e. that a ducts advantage is due to the reduction of propeller tip vortices as well as the hydrodynamic effects of the duct shape.

English (1967) produced a very useful report showing how momentum analysis can be used to analyse the performance effects on a ducted propeller when tip clearances are altered. The report is very mathematical but is understandable and has some experimental comparisons that prove the model is reasonable for small tip clearances ratios up to 0.02. Tip vortices are not accounted for, so it is unclear how the model performs at clearances above 0.02. He uses the example of a tanker and the effect of increasing the tip clearance. The graph in his example reaches a tip clearance ratio of 0.05 but if the example is reproduced it can be found that the model is not valid for values greater 0.06 since the performance drops below his own theoretical limit.

3.2 Critical review conclusions

In most proposed applications, circulation control technology has been used to augment lift force performance in existing devices e.g. aircraft wings and submarine stern planes. When augmenting lift performance in this way, extra complexity is required whilst maintaining the original structure (e.g. the original wing, rudder, stern plane etc.). The circulation control method therefore competes with other performance improvement devices that can also increase lift e.g. adding another flap or rudder, optimised airfoils and mechanical thrust vectoring.

It can be observed that in circumstances where circulation control has been used to *replace* existing technology (e.g. the NOTAR helicopter) it has been successful. In a similar way that circulation control has been used to replace the NOTAR helicopter's tail rotor, this project proposes to *replace* an AUV's control surfaces by using circulation control on the propeller duct.

Chapter 4. Basic Propeller Ducts

Before explaining the application of circulation control to a duct it is useful to explain the basic operation of a ducted propeller system. This chapter can be considered purely as an introduction to propeller ducts.

A propeller duct may accelerate or decelerate the flow, although this report only focuses on the accelerating type as seen in figure 4.1. Marine vehicles typically use the accelerating type, whilst decelerating types may be used on high speed naval devices such as torpedoes to reduce cavitation. An accelerating duct will generally increase efficiency performance on ships with a high thrust coefficient (Breslin, 1994). E.g. tug boats, trawlers, tankers, AUVs etc.

English (1967) carried out momentum analysis on a duct that derived the equations below. These can be used by first defining a power coefficient (similar to a thrust coefficient) and solving for K by finding the roots. Once K is determined the other values can be calculated.

Power Coefficient, $$C_P = \left[\sqrt{1+K} - \sqrt{1+K\cdot\left[1-(1-4\cdot\tau)\right]}\right]\cdot\sqrt{1+K}\cdot\left(\sqrt{1+K}+1\right)$$

Rotor Thrust Coefficient, $$C_{TR} = (1-4\cdot\tau)K$$

Total Thrust Coefficient, $$C_{TT} = 2\cdot\left[\sqrt{1+K} - \sqrt{1+K\cdot\left[1-(1-4\cdot\tau)\right]}\right]\cdot\sqrt{1+K}$$

Duct Thrust, $$C_{TD} = C_{TT} - C_{TR}$$

Propulsive Efficiency, $$\eta = \frac{2}{1+\sqrt{1+\frac{C_{TR}}{1-4\cdot\tau}}}$$

K = function of free stream velocity and velocity at duct exit.

τ = tip clearance/inside duct diameter at rotor tip.

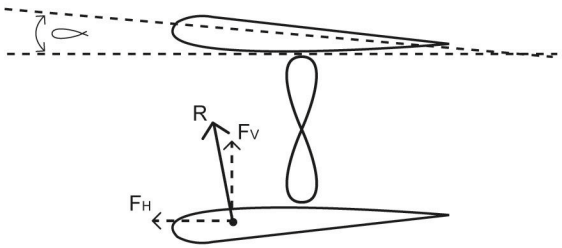

Figure 4.1. Accelerating duct.

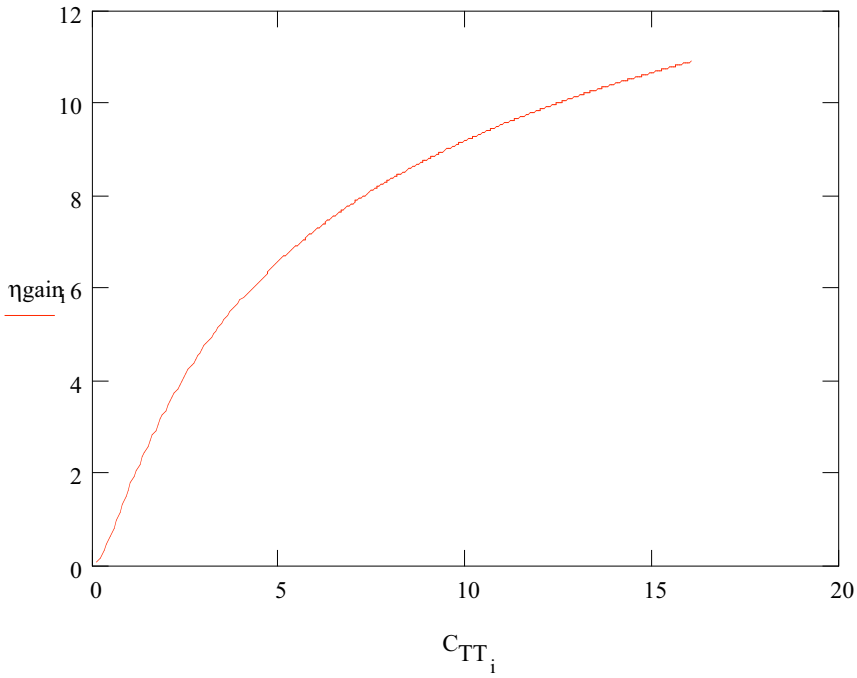

Figure 4.2. Effect of thrust coefficient on efficiency.

Figure 4.2 shows the effect on efficiency increase of a ducted propeller relative to an unducted propeller when the total thrust coefficient is varied. This shows there will be a minimum thrust coefficient where the advantage in efficiency is too small to justify the cost of fitting a duct. It also shows the maximum gain will reach a limit of around 13 % over a conventional unducted propeller.

The advantage of an accelerating ducted propeller comes from two separate mechanisms,

1. Reduction of propeller tip flow.
2. Negative angle of attack of the duct profile results in a forward thrust component.

The negative angle of attack of a typical duct causes a component of the normally vertical lift component to be directed forward (Olds, 2006). The resultant lift force (R) is marked on figure 4.1 and is shown split up into its horizontal (F_H) and vertical components (F_V). Using the equations from English (1967), the effect of the propeller tip clearance was investigated. Figure 4.3 shows the results. English also shows these results although only up to a tip clearance ratio of 0.05.

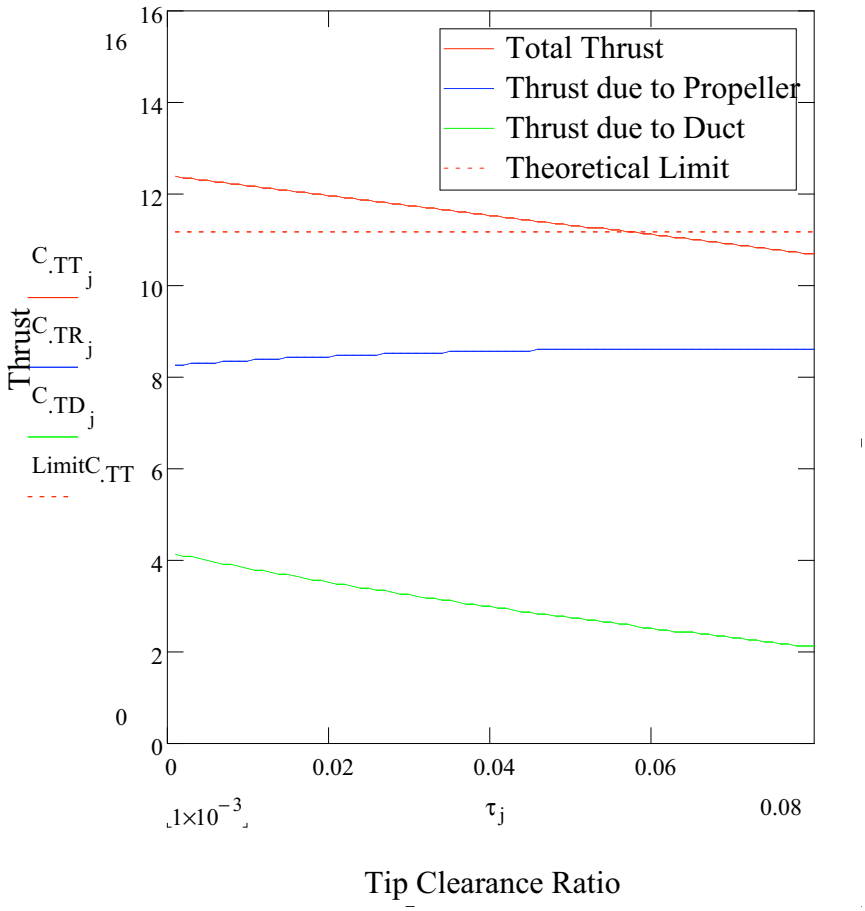

Figure 4.3. Effect of tip clearance ratio on thrust coefficients.

It can be seen from figure 4.3 that with zero tip gap (τ=0), the thrust generated by the duct (C_{TD}) will be responsible for increasing the total thrust (C_{TT}) by around 40 %. As the tip clearance ratio (τ) increases, the thrust due to the duct (C_{TD}) reduces until the theoretical limit is reached just after a tip clearance ratio of 0.05. At this value of tip clearance ratio, the tip gap can be considered infinitely big. However, it can be seen that even although the tip gap is "infinitely" big at this point, the duct (C_{TD}) still produces a forward thrust of 2.5. This force will only be due to the lift generated by the duct profile and its negative angle of attack. Therefore, it can be calculated that when the tip clearance ratio is zero, the duct profile lift force is responsible for about 60 % of the duct thrust (C_{TD}) and the effect of the propeller tip flow reduction produces about 40 % of the duct thrust. Above a ratio of 0.06 the model is not valid since the total thrust drops below the theoretical limit.

Chapter 5. Induced Lift Force

One of the aims of this project is to compare the induced manoeuvring lift force of the circulation control system to the traditional control surface system. This is done later in chapter 7. Before this comparison is possible, the induced lift force of the new system has to be calculated. This chapter describes the creation of a semi-empirical formula that can estimate the induced force generated by a ducted circulation control system given the duct's geometric and system parameters.

5.1 Creation of a semi-empirical lift force formula

In order to evaluate the force produced by a circulation control duct and compare it to a conventional control plane system it was necessary to create a semi-empirical formula describing the force produced. Most papers that test circulation control devices are augmenting lift so typically the original section is modified at its trailing edge with dimensions that are within the range of previous circulation control experiments. The new lift characteristics are then compared to the equivalent unmodified wing.

In the case of an unmodified duct on an AUV, the original duct has a net horizontal lift force of zero so it is meaningless to carry out a comparison with the unmodified duct. Since the proposed circulation control duct replaces the control planes, it is sensible to compare the force produced by the duct against the original control planes force. Therefore, a formula for calculating the induced lift force produced by the duct was deemed necessary. The following sections examine the factors that affect the induced manoeuvring lift force. These are then combined into a final induced lift force formula.

5.2 Basic jet momentum and lift force relationship

The relationship between the blowing jet momentum coefficient (C_μ) and the lift force coefficient (C_L) is well documented with many authors reporting a square root relationship (e.g. Englar, Rogers, Zhu, Ahn). As an example, figure 5.1 shows fitted curves (including the drag coefficient Cd) superimposed on the results presented by Imber (2004).

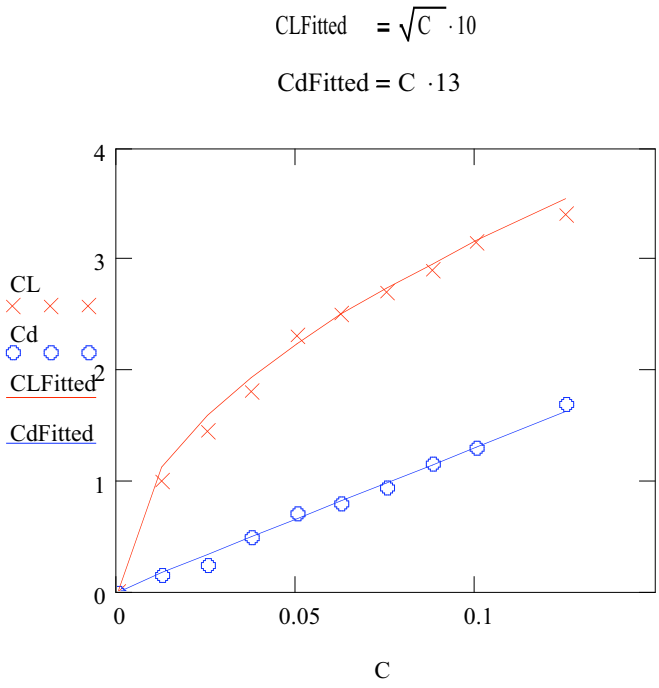

Figure 5.1. Fitted curves based on classic $C\mu/C_L$ relationship. (data from Imber, 2004).

This relationship forms the basis for the final lift force equation and it can be noted that there is also a coefficient that is present (10 in the above example). The jet momentum coefficient can be defined for 2D incompressible flow (chapter 3) as,

$$C = 2 \cdot \frac{h}{c} \cdot \left(\frac{V_j}{V_{inf.}} \right)^2$$

Therefore, the momentum coefficient is dependant on slot height, chord length, jet velocity and free stream velocity. It should also be noted that as the free stream velocity decreases the momentum coefficient becomes naturally large. This can effectively translate to large lift forces being generated at low vehicle speed. An example showing this basic trend is given in figure 5.2.

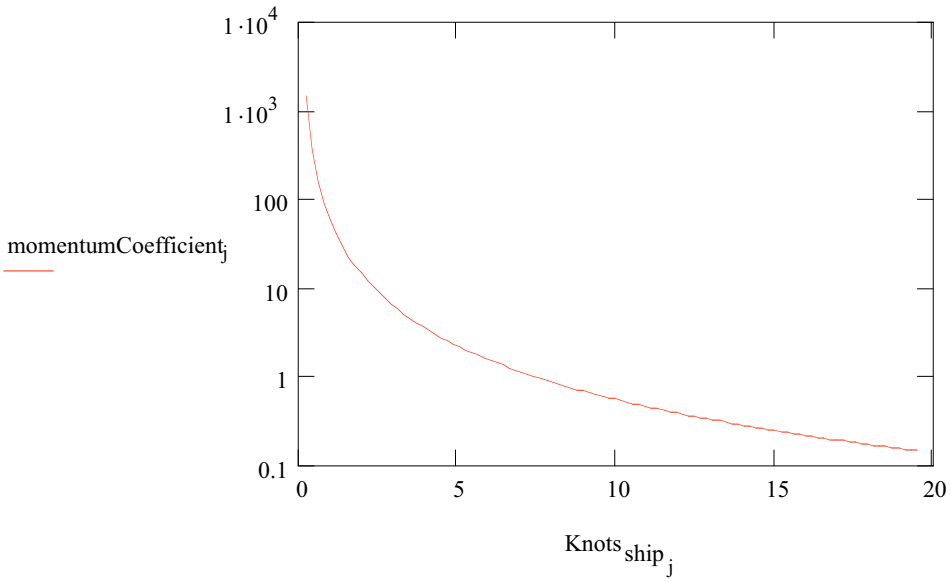

Figure 5.2. Effect of free stream velocity on momentum coefficient.

5.3 Effect of Coanda diameter

It is generally accepted that a round Coanda surface is best for jet attachment, however other surfaces such as ellipse curves will also work well (Englar, 1971). Only round surfaces are considered by the final lift equation due to a lack of available published test data.

Mason (2002) published the results of a series of experiments in which he varied the Coanda diameter (see figure 3.8 for the experimental setup) and measured the lift force produced. His results are shown in figure 5.3. Note that he uses a thrust vector coefficient (Cz) to represent force but this is closely related to the lift force coefficient (C_L).

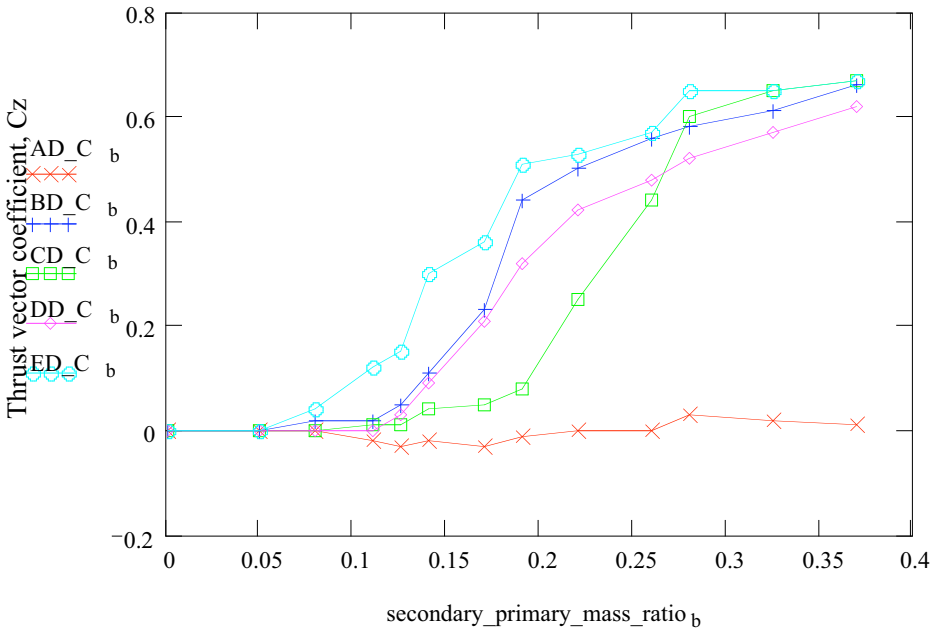

Coanda surfaces are expressed as (radius/chord length) and are, AD=0.017, BD=0.026, CD=0.034, DD=0.043, ED=0.052

Figure 5.3. Experimental data showing effect of varying Coanda diameter. (data from Mason, 2002).

It can be seen that the basic square root trend is still present in Masons results, however it is also clear that the graph has been shifted to the right. Mason does not offer a full explanation of this "dead zone". It can also be seen that the larger Coanda diameter E has a much reduced dead zone compared to diameter D. This may suggest that the dead zone is related to the Coanda diameter. However, the dead zone is not reported by other authors who have experimented with an airfoil in a non-static fluid flow. This suggests that the dead zone effect is primarily due to the speed of the external flow (which is zero in Masons experiment). Further experiments would be required to confirm this but since the dead zone is relatively small it will be excluded from analysis.

The range of diameters Mason used have been compared to the range of radius/chord ratios recommended by Englar (1971) for circulation control airfoils i.e. $0.02 < r/c < 0.05$. They are all within this range except the smallest diameter (AD) and it can be confirmed from figure 5.3 that this small diameter does not produce Coanda attachment.

Mason does not explain the effect of varying the Coanda diameter however an explanation is offered here. At an r/c ratio less than 0.02, Coanda attachment will not occur. Ratios between 0.02 and 0.043 offer good Coanda attachment but the performance is unpredictable. Above 0.043, it can be seen that the trend stabilises and is more predictable. Figure 5.4 shows the two "predictable" diameters. These were curve fitted and the relationship can be shown to be a simple bias term i.e.,

$$C_L = \sqrt{C - 0.25}\,0.35 + 0.54\,\text{CoandaDiameter} - 0.07$$

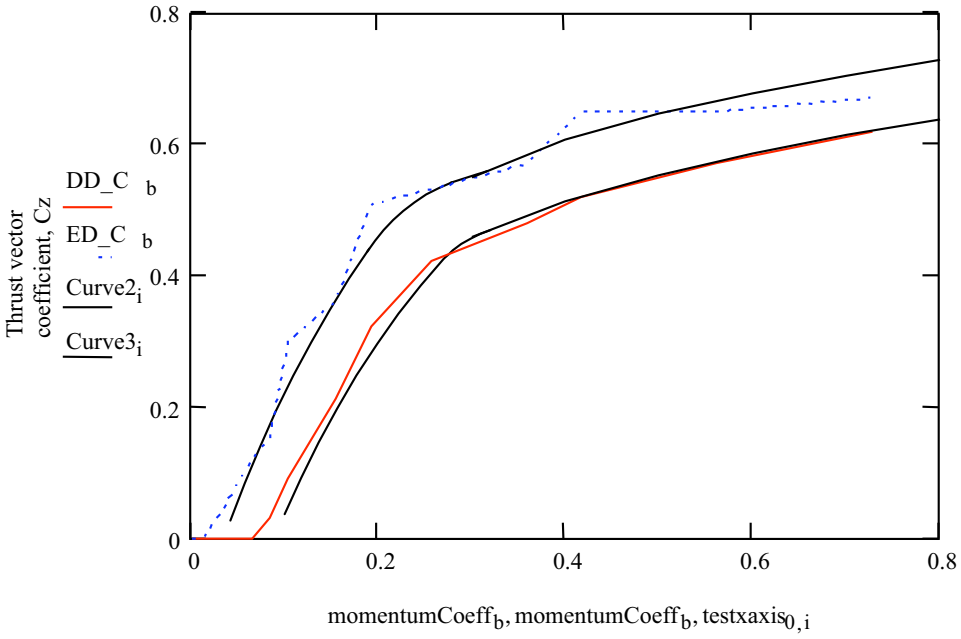

Figure 5.4. Fitted curves with varying Coanda diameter. (data from Mason, 2002).

The bias term is accurate for diameters at the upper end of the acceptable diameter range and it can be seen from the original results that if it is used in the range $0.02 < r/c < 0.043$, then it may under predict the lift force performance (e.g. diameter BD in figure 5.3).

5.4 Effect of slit length

Normally, when circulation control airfoils are tested, the jet slit is located straight along the trailing edge of the wing. In the proposed circulation control duct, the situation is more complex as the duct is circular. E.g. When the two right hand slits in figure 5.5 are activated concurrently, the action of the slits will induce a greater horizontal force effect near the horizontal axis compared to the slit region near the vertical axis.

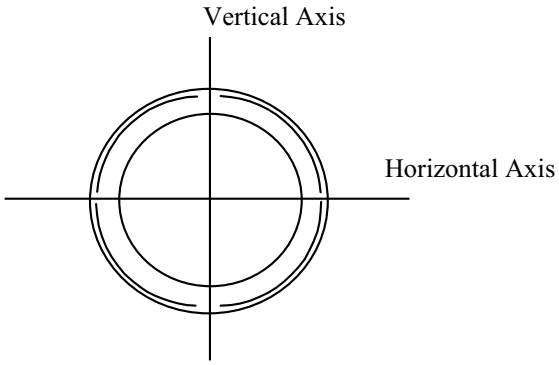

Figure 5.5. Rear view of circulation control duct.

Considering the same two slits, it can be seen that the circulation control acting at the horizontal axis point will only produce a horizontal force component. Everywhere else, a vertical component will also be produced. It can be seen that if the slits are symmetrical about the horizontal axis then the vertical components will cancel each other out (figure 5.6).

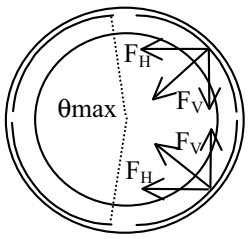

Figure 5.6. Rear view of circulation control duct, force components.

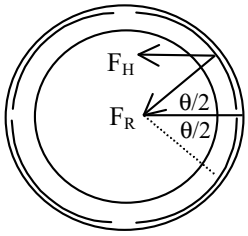

Figure 5.7. Rear view of circulation control duct, force components.

If one quadrant of the duct is considered, then integration of the horizontal force components round the slit yields in the total horizontal force,

$$F_{HT} = \int_0^{\theta max} F_R \cdot \cos\left(\frac{\theta}{2}\right) d\theta$$

For a simple horizontal manoeuvre there are two quadrants in operation, therefore the total force is,

$$F_{HT} = 2 \cdot F_R \cdot \sin\left(\frac{\theta max}{2}\right)$$

This shows there is a sinusoidal relationship between the slit length and the force produced. Englar (2004b) conducted an experiment on a half duct channel super-STOL aircraft wing (figure 3.7) and these results allow this formula to be tested. Englar varied the length of the slit and measured the lift force produced. These results are shown in figure 5.8. Note that the slit length is represented as an angle in degrees.

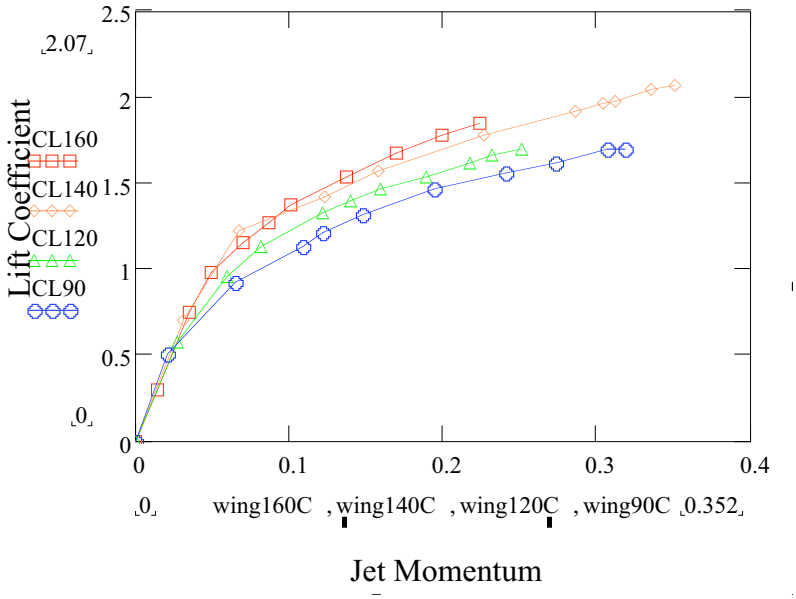

Figure 5.8. Experimental results of varying slit length. (Englar, 2004b).

These results were compared with the proposed sinusoidal formula and figure 5.9 shows the individual comparisons for different slit lengths. It can be seen that the function gives a fair estimate of the generated lift force. However, it can be seen with the smallest slit length the formula is less accurate (figure 5.9.d.). This would be expected since the medium is a fluid and as the slit length gets smaller, the force only acts on a small area of fluid near the duct axis. This will attempt to "split" the flow of water and lead to an increasingly complicated flow pattern.

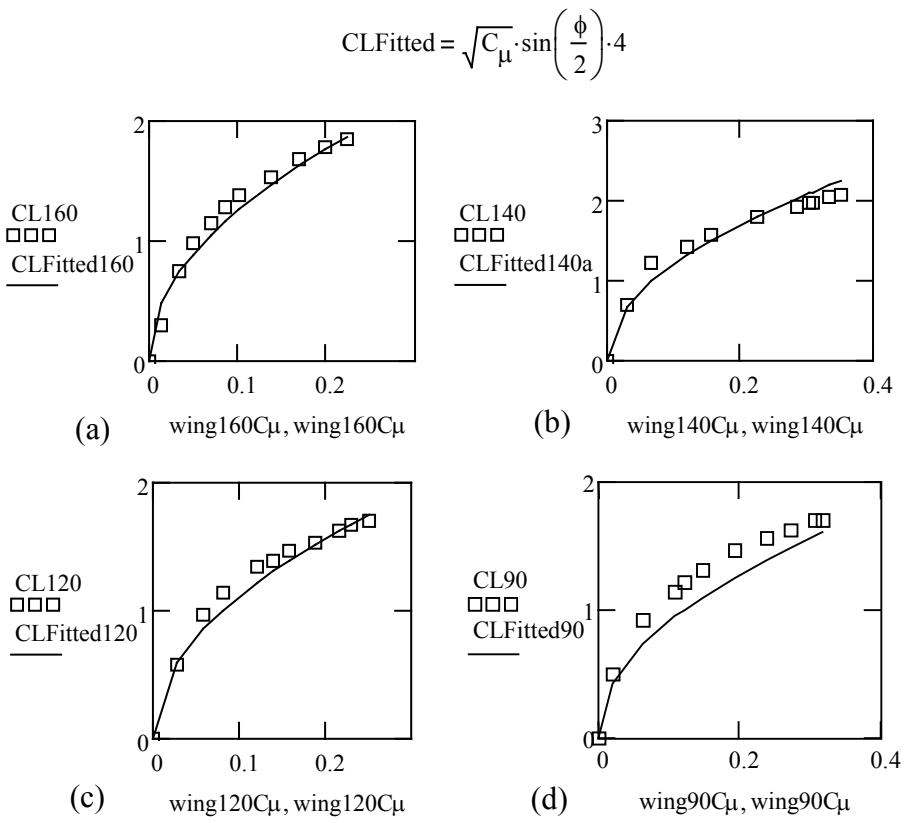

Figure 5.9. Theoretical slit length formula and experimental results (experimental data from Englar, 2004b).

5.5 Effect of propeller thrust

Since the wake of a propeller is complex, it is difficult to predict theoretically how the thrust and the circulation control will interact. Englar (2004b) tested a Super STOL aircraft circulation control system with the effects of propeller thrust. His configuration was essentially a half duct. The original results are shown in figure 5.10. The thrust coefficient is a function of force produced at the correct advance ratio, free stream velocity and wing area. Thrust coefficients tested had values of 0, 0.4, 1.0, 1.6 and 2.2. The Reynolds number was $16x10^3$. It can be seen that there is an impressive gain in the lift as a direct result of the propeller thrust.

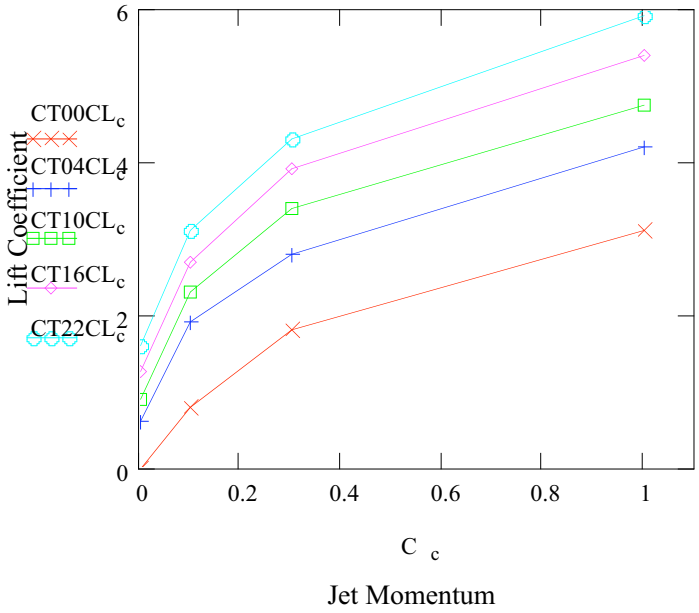

Figure 5.10. Effect of propeller thrust on lift coefficient. (Englar, 2004b).

It was discovered that increasing the thrust coefficient has two effects. One is to increase the bias of the lift curve and the other increases the gradient of the curve. These effects were captured in the formula,

$$C_L = \sqrt{C_{\cdot}} \cdot 3.94 \cdot 0.83 \cdot \left(\frac{C_T}{10} + 1 \right) + \sqrt{C_T} \cdot 1.4 - 0.05$$

Figure 5.11 shows the performance of this formula against the original experimental results. All the curves can be seen to provide a reasonably accurate match.

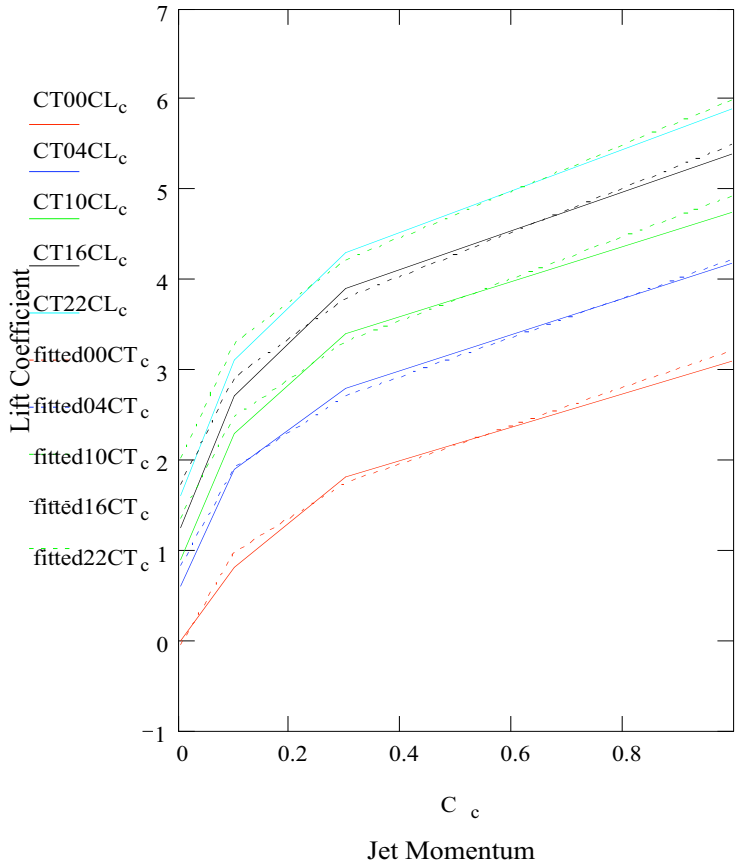

Figure 5.11. Comparison of curve fitted formula and original experimental results.

5.6 Effect of duct profile angle of attack

A less obvious influence of the modified duct is caused by the effect of the angle of attack of the duct profile. Normally a standard aircraft wing would use a positive angle of attack to increase the lift force. In a propeller duct such as the MARIN 19a, the standard duct generates a forward thrust component by having a negative angle of attack. Still considering a unmodified duct, figure 5.12 shows the effect on the lift force when a negative angle of attack is applied. If the angle of attack was zero then the lift force would act radially around the duct and have a zero net effect but the negative angle of attack causes a forward thrust component to be created from the lift force. The summation of the horizontal components of the lift force round the duct still results in zero.

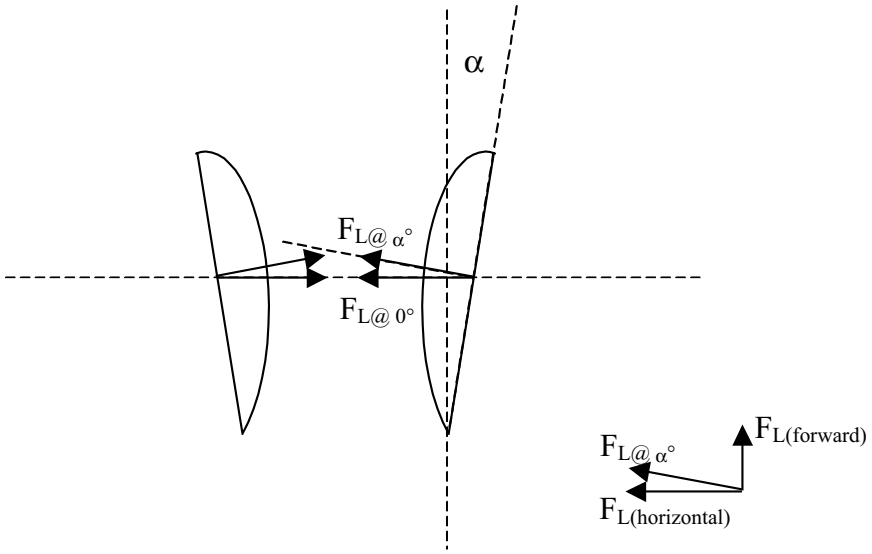

Figure 5.12. Cross section view of standard propeller duct showing effect of angle of attack.

When circulation control is applied to two adjacent quadrants of the duct, this causes one side of the duct to experience an increase in lift force ($F_{Linduced}$) thus unbalancing the previously net zero radial force. These components are shown in figure 5.13. Clearly, increasing the horizontal force is of primary importance there but it can also be seen that there is an induced increase in the forward thrust of the duct on one side. This extra forward thrust force is an unexpected consequence of applying circulation control to a duct and has not been reported in other circulation control applications.

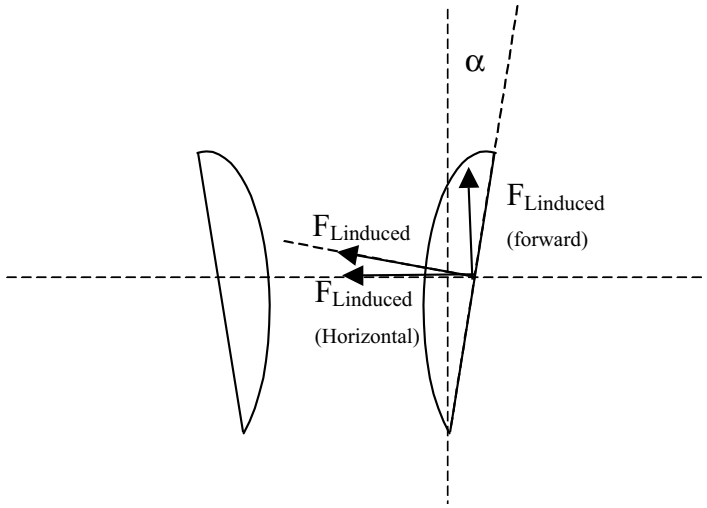

Figure 5.13. Cross section view of circulation control duct showing effect of induced forces when circulation control is activated on right hand side of the duct.

The horizontal manoeuvring force induced by the circulation control can be given by,

$$F_{Horizontal} = F_{Lresultant} \cdot \cos(\alpha)$$

The forward thrust induced by the circulation control can also be given by,

$$F_{Forward} = F_{Lresultant} \cdot \sin(\alpha)$$

This secondary forward thrust force will only occur on one side of the duct, therefore there will be an unbalance in forward force round the duct. The result of this is to create a turning moment that is beneficial to the manoeuvre.

5.7 Final semi-empirical formula for induced lift force coefficient

The previous sections have explained the effects of jet momentum (based on chord length, slot height, jet velocity and free stream velocity), the Coanda diameter, propeller thrust and negative angle of attack. These effects were combined and the final semi-empirical formula for the induced manoeuvring force can be defined as,

$$C_L = \sqrt{C} \cdot \left(4 \cdot \sin\left(\frac{\theta}{2}\right)\right) \cdot 0.83 \cdot \left(\frac{C_T}{10} + 1\right) \cdot \cos(\alpha) + \sqrt{C_T} \cdot 1.4 + 57.4\left(\frac{r}{c} - 0.0429\right) - 0.05$$

Chapter 6. Induced Drag Force

The previous chapter developed a semi-empirical formula for calculating the induced lift force (the manoeuvring force) of the circulation control duct. In a similar way, this chapter calculates the associated induced drag force of the duct. The induced drag force is important, as it is required for calculating the efficiency of the system. The formula developed for induced drag in this chapter is used in chapter 10 to compare the efficiency of the new system against the traditional control surface system.

6.1 Induced drag force

When an airfoil produces a lift force, this is only the vertical component of a resultant force that also includes a horizontal drag force component. Therefore it is natural when circulation control is applied to a wing that there is also an induced drag force created along with the useful lift force. Imber (2004) highlights that for Rogers's annular wing experiment, the drag force could be calculated using the classic lift-drag relationship used with conventional passive wings. i.e,

$$C_D = \frac{C_L^{\,2}}{\pi \cdot AR \cdot e}$$

The circulation control duct differs from Imber's annular wing since it has a much faster flow in the centre due to the propeller thrust. Englar's (2004b) Super STOL results were used as a basis for analysis because of the use of a propeller in his experiments. The drag measurements with different propeller thrust coefficients are shown in figure 6.1. Unfortunately the results include the propeller thrust force and the induced drag force. This is why most of the drag values are negative. Englar states that the drag and thrust cannot be reasonably separated however this has been attempted here.

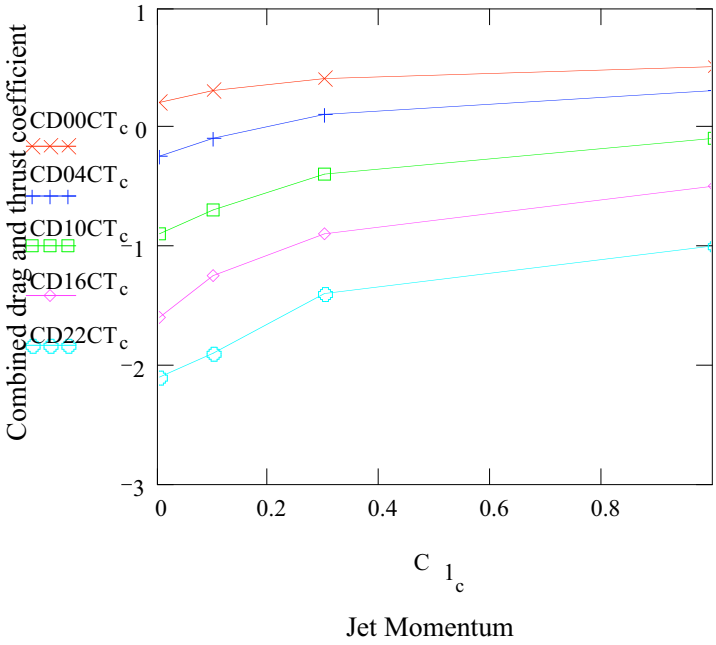

Figure 6.1. Effect of thrust coefficient and jet momentum on drag coefficient. (Englar, 2004b).

It can be shown that the drag curves shown in figure 6.1 can be estimated by,

$$C_D = \frac{C_L^{\,2}}{\pi \cdot AR \cdot e} + 0.1 \cdot \sqrt{C_{} } \cdot C_T - 1.1 C_T + 0.2$$

There are four terms influencing drag in this formula. The first term is the classic relationship as defined by Imber (2004). The second term describes the interaction between the jet blowing and the propeller thrust. This causes the graph to curve. The third term is the main thrust force (the negative C_T term). The final component represents the profile drag in the system. It is assumed that Englar's results for drag include the propeller, nacelle and the profile wing drag. The minimum drag was taken from the drag curve (in figure 6.1) at the point where the propeller thrust was zero and the jet blowing was zero. This gives a value of 0.2 which seems reasonable.

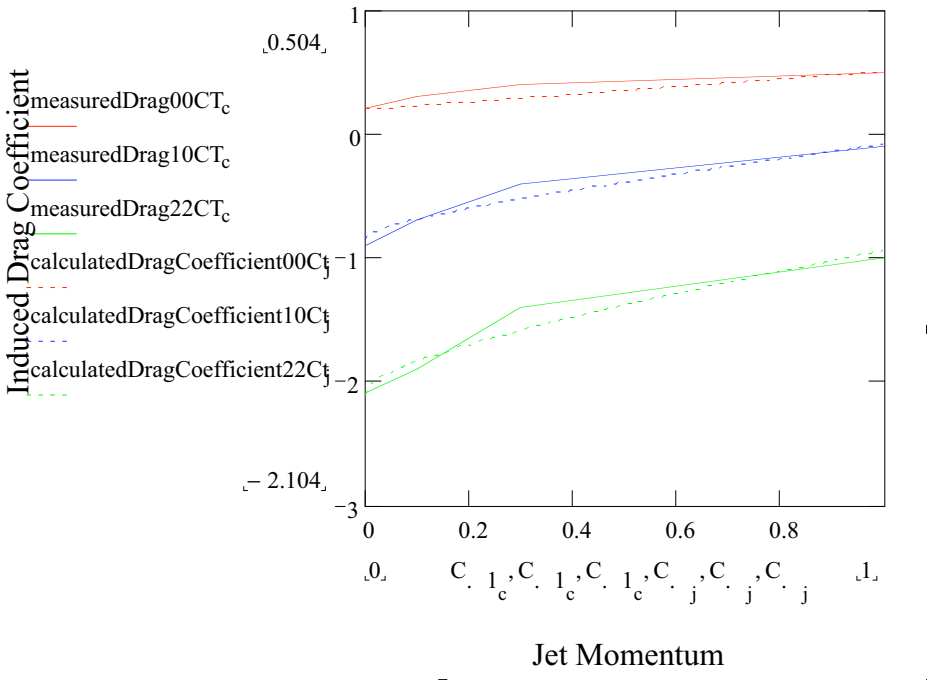

Figure 6.2. Comparison of computed drag coefficient against experimental results.

The drag formula is plotted in figure 6.2 and shows a reasonable match with the experimental results.

6.2 Final semi-empirical formula for induced drag force coefficient

Assuming that the assumptions made in the previous formula are correct, it is reasonable to remove the main thrust bias and the profile drag term to isolate the induced drag and its interaction with the propeller thrust. Therefore, the induced drag can be given approximately by,

$$C_D = \frac{C_L^{\,2}}{\pi \cdot AR \cdot e} + 0.1 \cdot \sqrt{C} \cdot C_T$$

This term is plotted in figure 6.3 and it can be seen that the negative components have been removed and that there is no positive bias due to the profile drag.

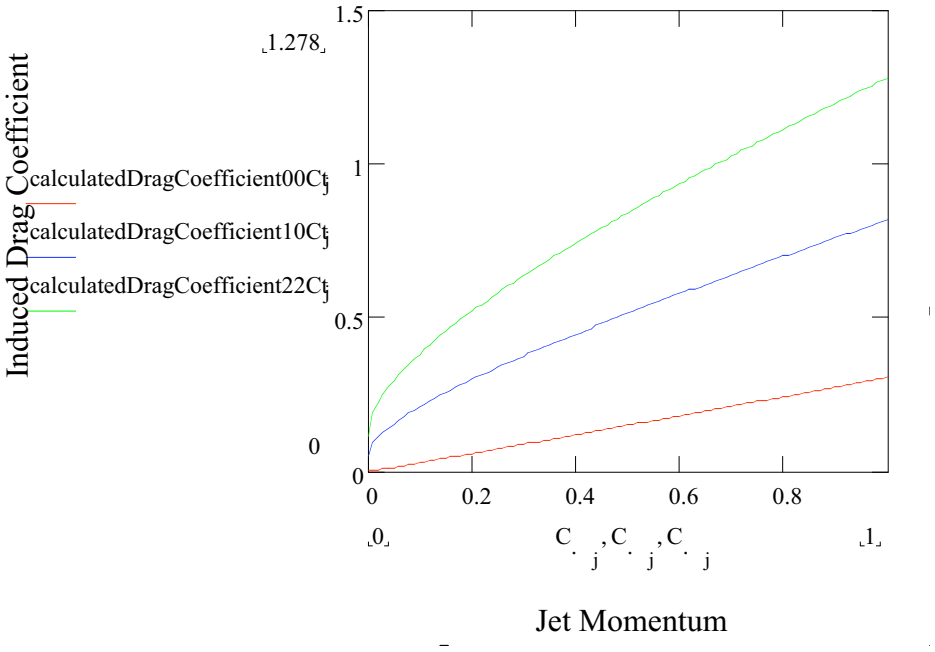

Figure 6.3. Calculated induced drag coefficient.

Chapter 7. Manoeuvring Force Comparison

One of the main aims of the project is to compare the manoeuvring force developed by the new circulation control duct against the traditional AUV control surfaces. This is done in this chapter. Chapter 5 described a formula for calculating the induced lift force of a circulation control duct and this is used in this chapter to calculate the comparison. It was also identified in chapter 5 that there is an additional secondary forward thrust force generated by the duct's negative angle of attack and the circulation control. This secondary force is also calculated in this chapter.

In order to compare the force performance of the new duct system against a traditional control surface system, an example AUV was chosen due to its suitability for the new system. This was a U.S. Navy "Seahorse" AUV that uses a ducted propeller. It is pictured in figure 7.1.

Figure 7.1. U.S. Navy's Seahorse AUV. (NAVOCEANO, 1999)

The Seahorse AUV is 8.5m long, has a 97cm diameter and a weight of 5 tonnes.

Figure 7.2. U.S. Navy's Seahorse AUV control planes and propeller system. (NAVOCEANO, 1999)

7.1 Traditional AUV control surface performance

An AUV control surface system such as the type used on the U.S. Navy Seahorse operates partially in the complex propeller flow and therefore its performance will be different from control surfaces operating in open water. Lewis (1989) shows that lift performance can be improved since the stall angle may be extended to higher angles and the stall characteristics less drastic. A widely known formula for estimating rudder lift force and drag is given by Lewis (1989) and Bishop (1982),

$$C_L = \frac{0.9 \cdot 2 \cdot \pi \cdot a}{57.3 \cdot \left(\cos(A) \cdot \sqrt{\frac{a^2}{\cos(A)^4}} + 4 + 1.8 \right)} + \frac{C_{Dc}}{a} \cdot \left(\frac{\alpha}{57.3} \right)^2$$

$$C_{Drudder} = C_{do} + \frac{C_L^{\,2}}{\pi \cdot AR \cdot e}$$

Only induced lift force is analysed in this chapter's calculations, so C_{do}, the static drag, is set to zero. Figure 7.3 demonstrates the effect of changing the control surface angle. The useful deflection angle range is dependant on the control surface shape, size and specific installation but a typical maximum deflection angle for a survey type AUV is around 7 degrees (Merry, 1996). This results in a lift coefficient of 0.39.

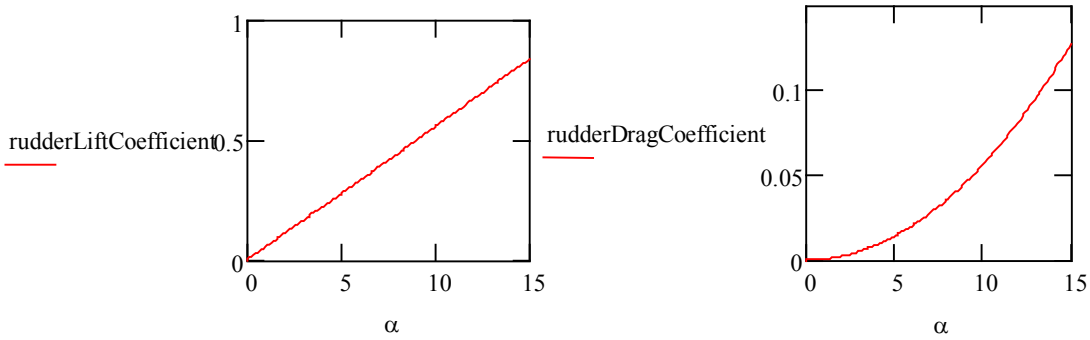

Figure 7.3. Effect of angle of attack on induced lift and drag coefficients for a traditional AUV control surface system.

During the force comparison calculations in this chapter, the water velocity that the control surfaces experienced was set to 1.3 times the AUV speed. This figure is normally used when estimating rudder force (Lewis, 1989). In the force comparison in the next section, the control surfaces always operate at their maximum lift force value (i.e. operating at 7 degrees).

7.2 Circulation control duct manoeuvring force comparison

The induced lift force of the circulation control duct was calculated using the formula derived in chapter 5. The force was calculated on the basis of modifying the duct already used on the Seahorse AUV. i.e. diameter of 0.7 m, chord length = 0.23 m, duct angle of attack = -10 degrees (assumed), jet blowing around 180 degrees, Coanda radius/chord length = 0.010, slot height = 0.58 mm, V_{jet} = 6 m/s, propeller thrust coefficient K_T = 0.5. Other assumptions are given in appendix B including

conversion of the thrust coefficient K_T to C_T. The maximum AUV speed was set at 6 Knots and the blowing momentum adjusted until the force produced by the new system was at least equal to the magnitude of the control plane force. It is assumed that the modified duct is split up into four slot blowing quadrants and two quadrants would be activated concurrently with circulation control to produce a simple one-axis manoeuvre.

The final induced force comparison is shown over the AUV's full speed range in figure 7.4. Lower speeds are shown in figure 7.5. Note that a logarithmic scale is used in these two figures. The percentage improvement is shown in figure 7.6.

It can be seen that the circulation control system is capable of generating much higher forces than the conventional control surfaces at low speed. At 1 Knot, the force is improved by 600 %. This gain reduces when the same jet momentum level is maintained and the AUV speed increased. This performance improvement may seem like a large amount but it should be noted that a passive device is being compared against an active force producer. Rogers (2004) reports a tenfold force gain at 1 Knot when testing a circulation control submarine stern plane against a standard unmodified control surface. Roger's analysis differs slightly as it was based on a single submarine stern plane in open water whereas this analysis is based behind the propeller wake and uses two control surfaces for comparison. In addition, the circulation control surface proposed by this report is annular. It has already been indicated that the complicated propeller wake tends to increase the lift performance of both the new circulation control duct (chapter 5) and traditional control surfaces (section 7.1).

Above 6 Knots, the conventional control surfaces offer superior performance although this point was fixed by the jet momentum because 6 knots is the Seahorse AUV's maximum speed. The lift force generated by the circulation control duct could be increased further by increasing the jet momentum.

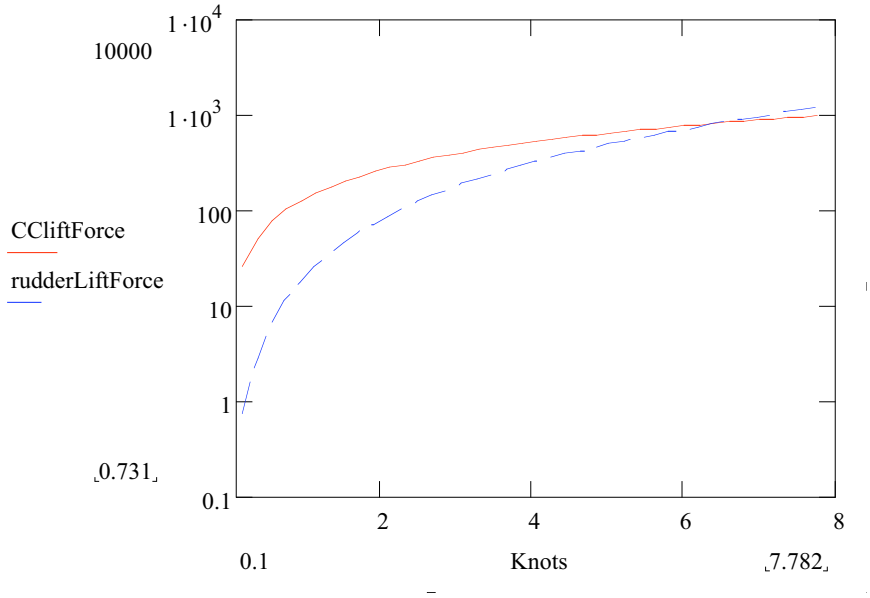

Figure 7.4. Comparison of the circulation control duct and traditional control surface forces for the Seahorse AUV.

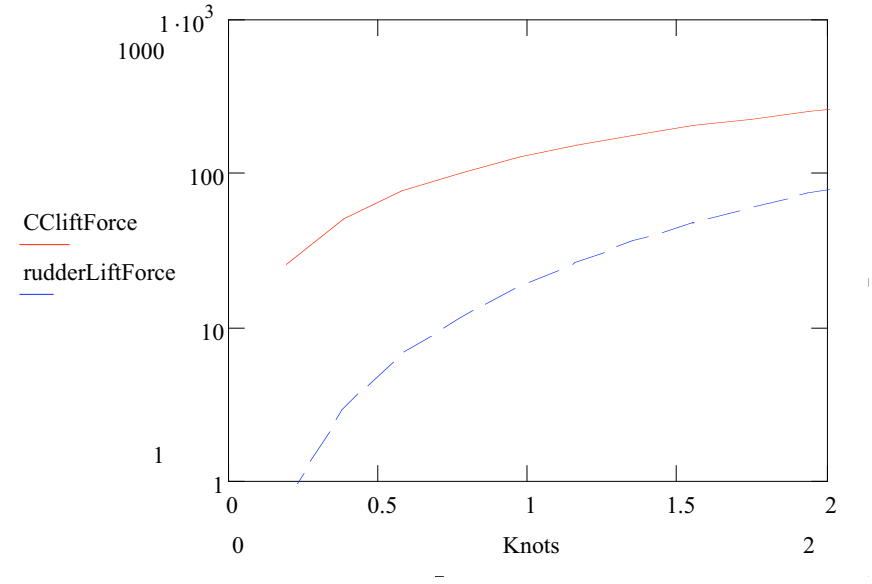

Figure 7.5. Comparison of the circulation control duct and traditional control surface forces for the Seahorse AUV. (Lower speeds).

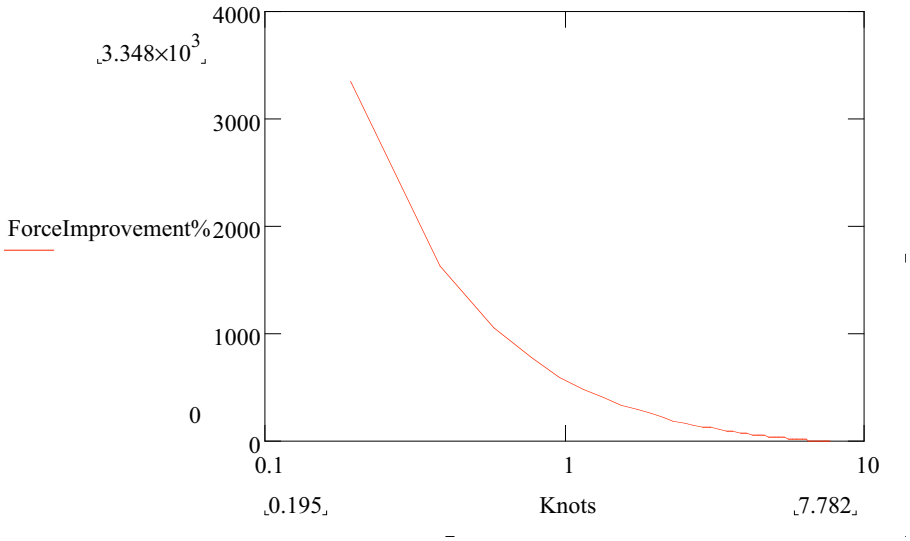

Figure 7.6. Percentage force improvement for the Seahorse AUV.

7.3 Secondary forward thrust force

It was explained in chapter 5 that as a result of the duct's negative angle of attack there will be an unbalanced forward thrust force generated at one side of the duct during jet blowing. This extra force has been calculated for the Seahorse AUV example and is shown in figure 7.7 relative to the main manoeuvring lift force. This secondary force has a magnitude of 14 % of the basic manoeuvring force produced by the circulation control duct at 6 Knots and will be beneficial for the manoeuvre. This force is not a direct horizontal force but is a turning moment forward about the duct. In reality, it is expected that this force will not substantially improve manoeuvring. Normally, ships with two propellers do not use them independently to steer since it results in poor manoeuvring performance (Lewis, 1989). It would be thought that this situation would be comparable.

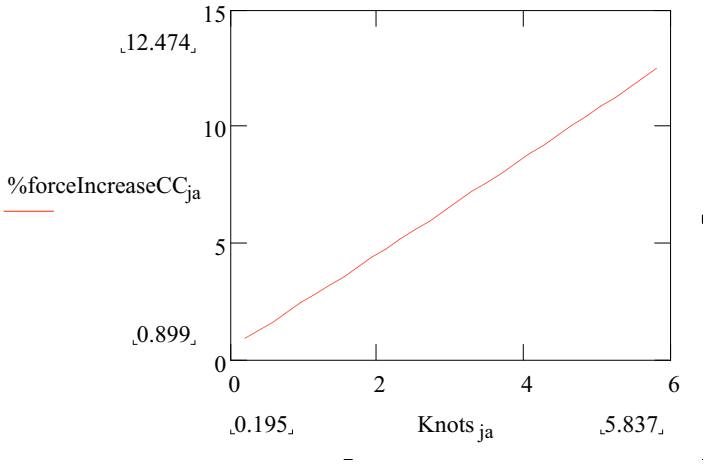

Figure 7.7. Induced forward thrust force relative to the manoeuvring lift force.

Chapter 8. Modified Duct Profile

A main aim of the project was to specify the profile shape and structural changes required to be made to the original duct in order to implement the circulation control technique. These modifications are described in this chapter.

The original profile of a common accelerating duct (a MARIN 19a) is shown in figure 8.1. The specific profile of the Seahorse AUV's duct profile is not known but it is assumed that it is similar to the MARIN 19a. A recommended modified profile to implement circulation control is shown in figure 8.2. The new duct will require modification in 4 main areas.

1. A jet blowing slot is added tangentially to the trailing edge. This is split into four quadrants to enable the force to be directed in a similar manner to a traditional four control plane system on an AUV. For a basic manoeuvre, two quadrants can be activated concurrently so that almost 180 degrees of the duct produces a force. Figure 5.5 shows the four slits at the aft end of the duct. Englar (1971) gives a recommended range for slot height as $0.0025 \geq (\text{height/chord}) \geq 0.0005$. Rodgers (2004) also discusses jet velocity. Essentially, these values are not critical and it is the overall jet momentum value that is of primary importance.

2. The trailing edge should be increased in diameter. The standard 19a trailing edge diameter is slightly below the threshold for Coanda attachment. The minimum radius/chord length ratio is give by Englar (1971) as 0.02 and the standard 19a has a value of 0.019. The minimum ratio agrees with Mason (2002) who demonstrated that a system with a ratio of around 0.017 does not result in attachment but 0.026 did. Figure 8.2 shows a modified section with the diameter increased by a small amount to ensure attachment. Figure 8.3 shows a duct with the diameter doubled. This large increase would bring the ratio into conformance with most previous circulation controlled airfoil's radius/chord ratios. Table 8.1 shows typical values used by other authors. A larger Coanda diameter generally results in a higher C_L/C_μ ratio but will

also likely result in greater profile drag. A marine vehicle will not spend all its time manoeuvring heavily, so it would be preferable to keep the diameter as small as possible to minimise the profile drag. Therefore the smaller ratio of 0.02 used in figure 8.2 would likely be the best choice (subject to a prototype evaluation and test).

3. Rodgers (2004) reports that excessive jet turning will occur at high momentum coefficients. This causes premature "jet blowing stall" when the high momentum jet wraps round the Coanda surface by 180 degrees. High momentum rates occur when a high level of jet blowing is used. They also occur naturally when the vehicle speed is low, although it is not thought that this excess turning situation would affect performance and this is confirmed by Mason's (2002) static experiments. Rogers uses a perfectly round trailing edge and dual slot blowing to prevent excess turning (figure 8.4) but other authors such as Englar (2004b) have modified the trailing edge geometry to prevent this occurring. The arrangement proposed in figure 8.3 has modified the geometry. This avoids the added complexity of dual slot blowing. A suitably small secondary diameter is used at the trailing edge to prevent Coanda attachment past 90 degrees. In reality, it requires high powers to operate with high levels of jet blowing and operation would not normally be required or recommended at these levels due to efficiency issues. Therefore the secondary diameter is unlikely to be required in most applications.

4. The profile shape may require modification at a place other than the trailing edge to maintain the duct's original profile lift coefficient. By modifying the trailing edge diameter severely as in figure 8.3, it can be seen that the lower part of the section has effectively been made longer. This may increase the lift. Therefore, to reduce the lift back to its original level, the profile shape requires extra modification. A dotted line in figure 8.3 towards the leading edge suggests a suitable change. Physical model testing is required to confirm whether this modification is necessary.

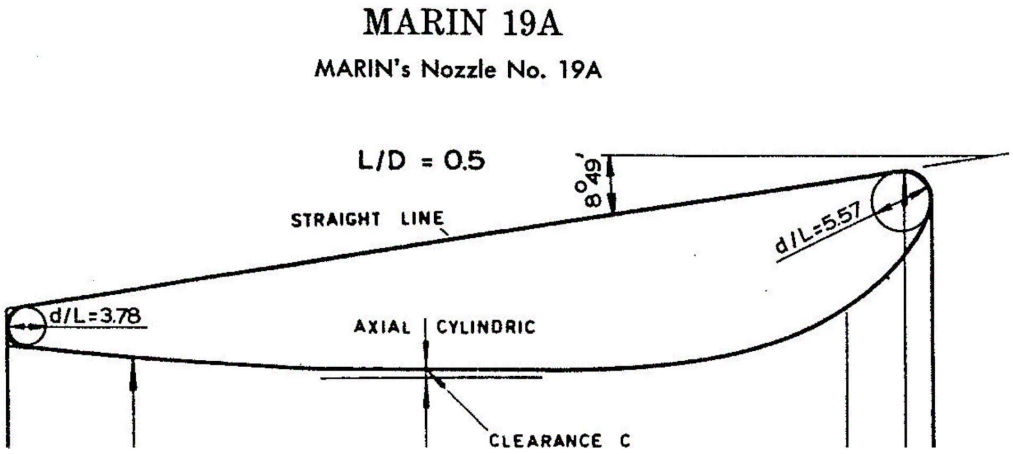

Figure 8.1 Original MARIN 19a duct section (Oosterveld, 1972).

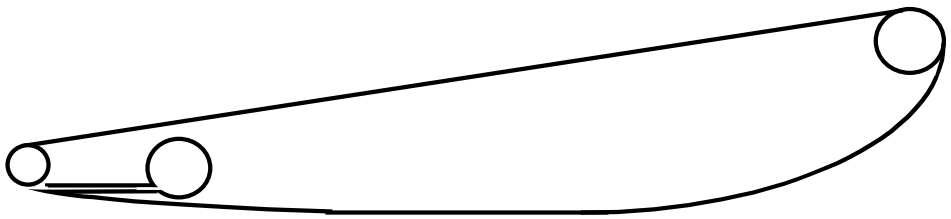

Figure 8.2 New modified MARIN 19a duct section – small diameter.

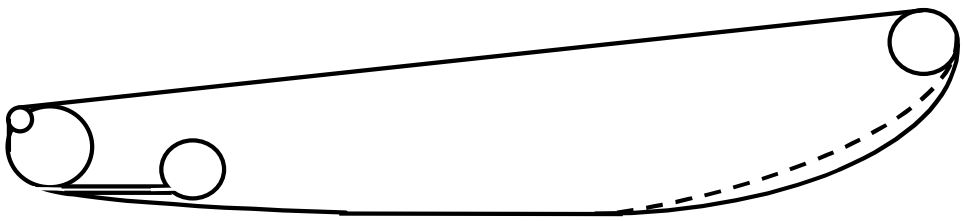

Figure 8.3 New modified MARIN 19a duct section - large diameter.

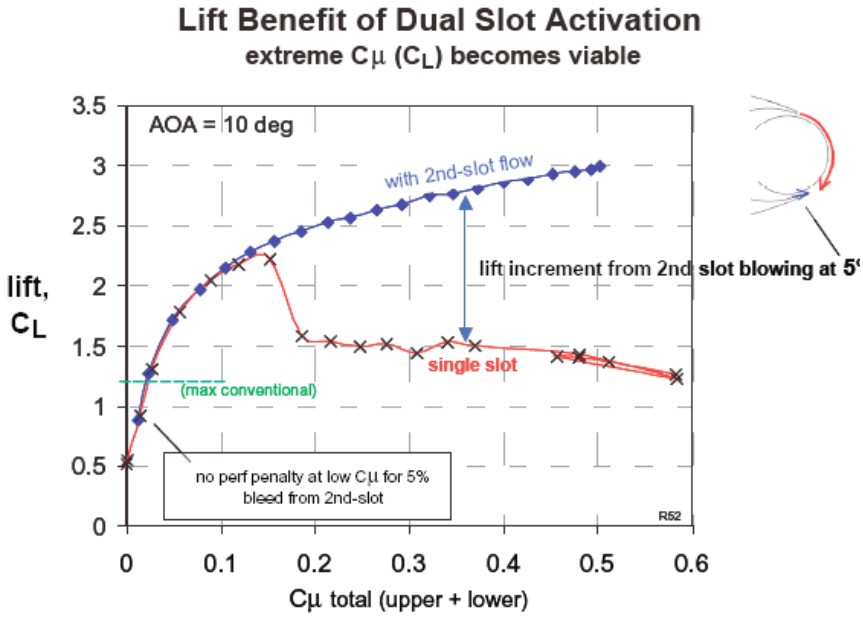

Figure 8.4. Dual slot blowing method. (Imber 2004).

Author	Approximate Coanda Radius/Chord Length
Kind and Maull (1968)	**0.0364**
Englar (1971)	**0.0384**
Zhu and Xianfu (1995)	**0.0253**
Rogers (2004)	**0.0428**
Englar (2004)	**0.0429**
Original MARIN 19a section	**0.0190**
Modified MARIN 19a section - large diameter	**0.0429**
Modified MARIN 19a section - small diameter	**0.0200**

Table 8.5. Approximate Coanda radius/chord length ratios.

Chapter 9. Profile Drag

A major aim of the project was to compare the efficiency of the circulation control duct against the conventional AUV control surface system. The efficiency comparison is covered in the next chapter but before this is done, the profile drag of the modified duct has to be calculated. This chapter attempts to estimate the profile drag. The profile drag is important; the previous chapter identified the requirement that the modified duct should have a rounded trailing edge with a possible increase in diameter. This modified trailing edge will likely increase the profile drag and reduce the efficiency.

It was assumed in chapter 8 that the original profile used on the Seahorse AUV is a MARIN 19a profile (figure 8.1) and this was therefore the starting profile for analyse. An attempt was made to calculate the profile drag using a program called Javafoil (Javafoil, 2006). This estimates airfoil performance using a potential flow, high order panel method. Unfortunately, the performance of the program's analysis was found to be unreliable due to separation of flow around the airfoil. Flow separation by the airfoil was caused by the angle of attack of the original unmodified section and also the non-tapering blunt trailing edge. Figure 9.1 shows the flow separation of the original MARIN 19a profile and reveals that the fixed angle of attack (-10 degrees) causes the majority of the separation (and thus profile drag) at speed.

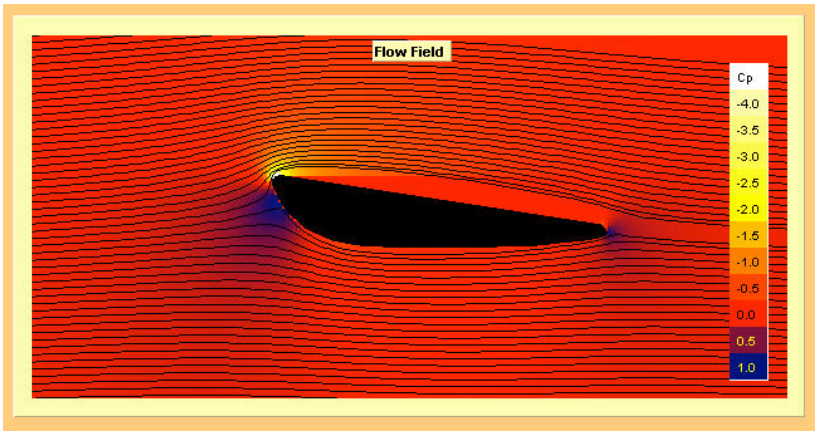

Figure 9.1. Flow separation of the original MARIN 19a section at Re=10x10^4. (generated using Javafoil).

The original MARIN 19a section has a relatively high drag coefficient of 0.17 (Olds, 2006) and this is mostly due to the leading edge flow separation as demonstrated in figure 9.1. Therefore it can be assumed that modifying the trailing edge by increasing the diameter slightly (as in figure 8.2) will result in a negligible increase in drag coefficient. If larger trailing edge diameters were to be used or if the system was to be fitted to a different duct profile then the drag coefficient would have to be calculated using tank testing or CFD analysis and factored into the efficiency calculations considered in the next chapter.

Recently, manufacturers claim to have improved the drag coefficient of ducts with improved foil designs and these now tend to be fitted instead of the traditional MARIN 19a and 37 profiles. Olds claim an efficiency of 0.01 for their Rice-speed design (figure 9.2). This seems reasonable for a typical foil without leading edge separation.

Figure 9.2. Rice-Speed nozzle section. (Olds, 2006).

With these optimised foil designs, the leading edge separation does not dominate the drag and fitting a suitable circulation control diameter to the trailing edge has increased drag implications on the original profile drag coefficient. Although this report focuses on modifying the MARIN 19a nozzle with circulation control, an indication of the profile drag increase for more modern nozzles can be seen from a modified NACA 0012 section by Lowry (1956). The section is shown in figure 9.3.

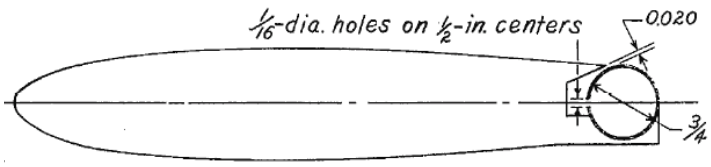

Figure 9.3. Jet flap airfoil based on a modified NACA 0012. (Lowry, 1956).

Jet flap technology was a predecessor of circulation control techniques and Lowry's experiments were based upon a symmetrical NACA 0012 with the trailing edge modified. The drag coefficient of this airfoil was approximately 0.8 at $Re=25x10^4$ whereas an unmodified NACA 0012 has an estimated drag coefficient of 0.075 at $Re=25x10^4$ (calculated using Javafoil). This represents a tenfold increase in drag although it should be noted that this jet flap airfoil uses a large trailing edge diameter akin to the profile in figure 8.3 that was not recommended.

Chapter 10. Efficiency Comparison

This chapter compares the efficiency of the new circulation control system against the efficiency of a traditional AUV control plane system. This comparison is a major aim of the project and is particularly important on an AUV marine vehicle due to the limited power available from the onboard power source. The power required to produce the circulation control jet is also calculated to aid understanding.

The efficiency of a lift producing device (airfoil, duct, control surface etc.) can be described using the lift/drag ratio (Englar, 1971). In this chapter, the lift/drag ratio is calculated for the traditional AUV control surface system and also for the new circulation control duct system. They are then compared.

10.1 Efficiency of a conventional AUV control plane

The efficiency of a conventional duct and control surface based system can be defined as the lift/drag ratio of the system,

$$\frac{C_L}{C_D} = \frac{C_L}{C_{Dp\_Duct} + C_{Dp\_Rudder} + C_{Di\_Rudder}}$$

Where,

C_L = induced lift force coefficient

C_D = total drag force coefficient

The drag in this control surface based system consists of,

1. C_{Dp_Duct}, the duct profile drag coefficient.
2. C_{Dp_Rudder}, the control plane profile drag coefficient.
3. C_{Di_Rudder}, the control plane induced drag coefficient.

The induced lift coefficient and induced drag coefficient were calculated using the equations defined in chapter 7. The profile drag of conventional airfoils are well documented and the comparison used a NACA 0015 profile. The profile drag of the original duct was also known as it was a standard MARIN 19a duct.

The lift coefficient used in the equation only includes lift generated by the control plane. Profile lift generated by the duct is assumed unchanged in the new system therefore it can be excluded from all analysis. The power required to move the control surfaces is not included in the calculation since it is manoeuvre dependent.

10.2 Efficiency of new circulation control duct system

The efficiency of the new circulation control duct system can be defined as,

$$\frac{C_L}{C_D} = \frac{C_L}{C_{dp\_Duct} + C_{di\_Duct} + C \cdot \frac{V_j}{2 \cdot V_{inf}} + C \cdot \frac{V_{inf}}{V_j}}$$

The drag force used in the equation above is defined as,

$$D = D_{dp\_Duct} + D_{di\_Duct} + \frac{PumpPower}{V_{freestream}} + D_{Inlet}$$

This drag term consists of,

1. C_{dp_Duct}, the duct profile drag coefficient.
2. C_{di_Duct}, the duct induced drag coefficient (generated by the circulation control).
3. $(PumpPower/V_{freestream})$, the jet pump power expressed as a drag coefficient.
4. D_{Inlet}, the pump inlet loss expressed as a drag coefficient (Englar, 1971).

The induced lift force coefficient was calculated using the semi-empirical lift force formula (chapter 5). The induced drag coefficient was calculated using the related induced drag formula (chapter 6). The duct profile drag was assumed to be the same as the original MARIN 19a profile drag (chapter 9).

10.3 Efficiency comparison

The efficiency comparison was based on the U.S. Navy's Seahorse AUV and used the two equations for efficiency developed above. The direct comparison can be seen in figure 10.1 and the percentage change in efficiency is shown in figure 10.2.

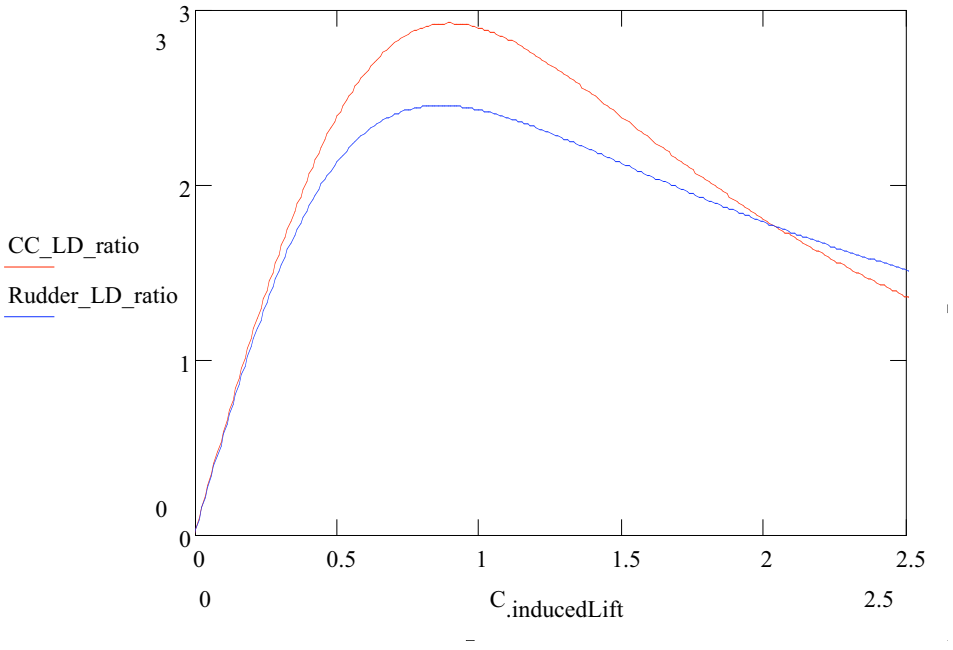

Figure 10.1 Efficiency of control plane system and circulation control duct system.

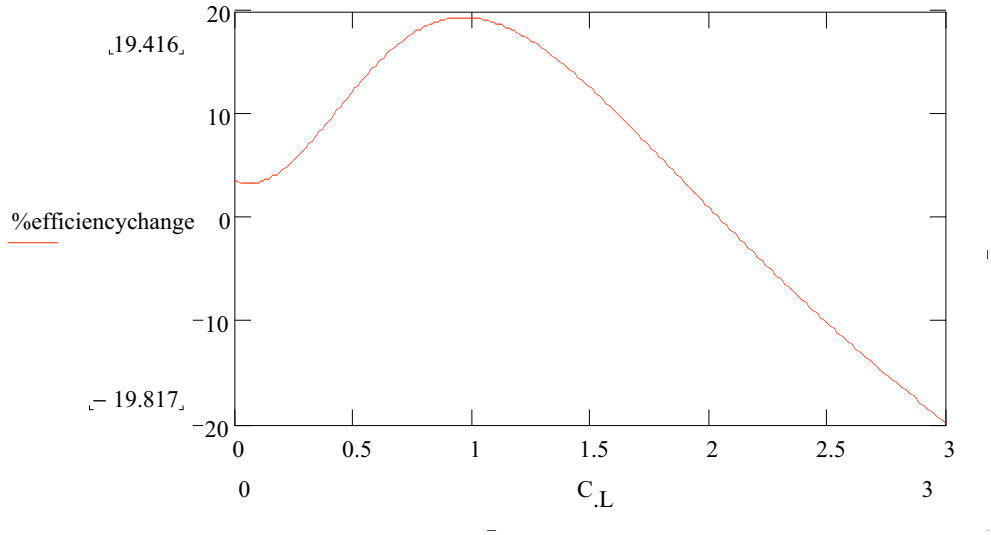

Figure 10.2. Efficiency of circulation control duct system relative to a conventional control surface system.

The circulation control duct used in the comparison was based on a MARIN 19a with the trailing edge diameter unchanged i.e. similar to the section in figure 8.2. This allowed the known profile drag of the original duct to be maintained. The trailing edge diameter (r/c =0.019) of the original 19a duct almost meets the Coanda diameter requirements (min r/c =0.02) so Coanda attachment would still likely occur. The induced lift performance was assumed to be working at an effective higher diameter (r/c=0.0429) since the duct trailing edge diameter is operating in the unpredictable Coanda diameter range (chapter 5).

It can be seen from figure 10.2 that there is a small increase in efficiency at zero and very low values of lift coefficient. This is due to the circulation control duct system having no rudder. Therefore, the profile drag of the rudder has been eliminated.

The efficiency of the circulation control system then increases and peaks at a lift coefficient of 1. It would be thought that the circulation control system would always be less efficient due to the power required from the jet pump. However, this is not always the case and it can be seen from figure 10.3 that the induced drag of the control plane system is actually greater than the circulation control system. This is

due to the effects of the aspect ratio and the Oswald efficiency factor. The control plane has greater induced drag because of the tip flow effects. The duct has a higher aspect ratio (AR = 3.13) and higher Oswald efficiency factor (e = 1.17) since it is annular and therefore has no tip flow. This makes it a more efficient lift producer.

Above a lift coefficient of 1, the efficiency gains of the circulation control duct system starts to decline. This is caused by the rising power requirements of the jet pump. It can be seen in figure 10.4 that above a lift coefficient of 0.6, the equivalent drag produced by the pump becomes greater than the induced drag and therefore dominates the performance.

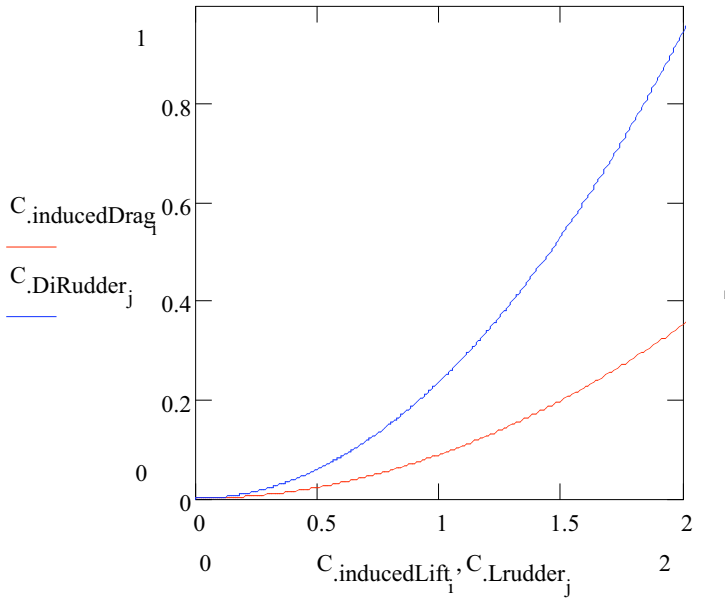

Figure 10.3 Comparison of control plane and circulation control duct induced drag.

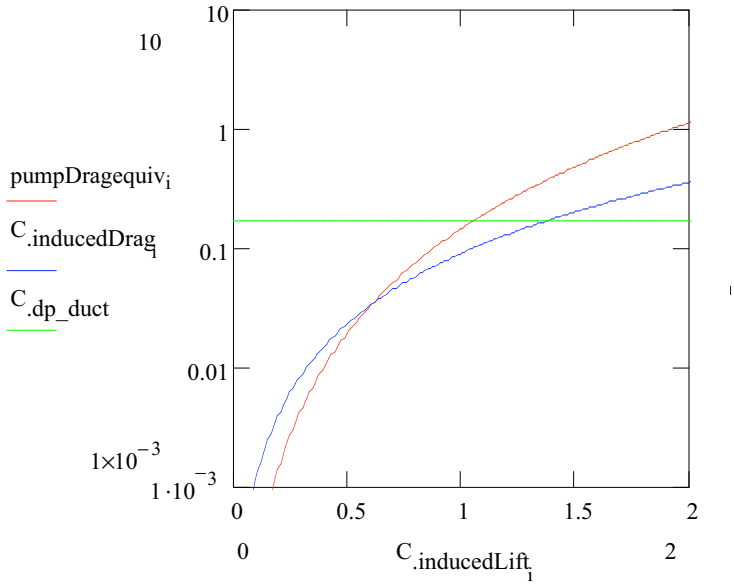

Figure 10.4. Drag sub-components in circulation control duct system.

The efficiency calculations that have been carried out are a modified version of the type proposed by Englar (1971). Englar also shows some lift/drag efficiency comparisons with experimental results. These are shown in figure 10.5. The experiments used straight airfoils (as opposed to the higher performance annular duct used here) and were carried out in a wind tunnel. In particular, a NACA 0012 was compared against a 20 % thickness, 5 % cambered ellipse that uses circulation control. This particular comparison is reasonably similar to the comparison that was carried out with the modified duct. The results are similar but with a lower efficiency that can be explained by the lower aspect ratio and Oswald efficiency factor.

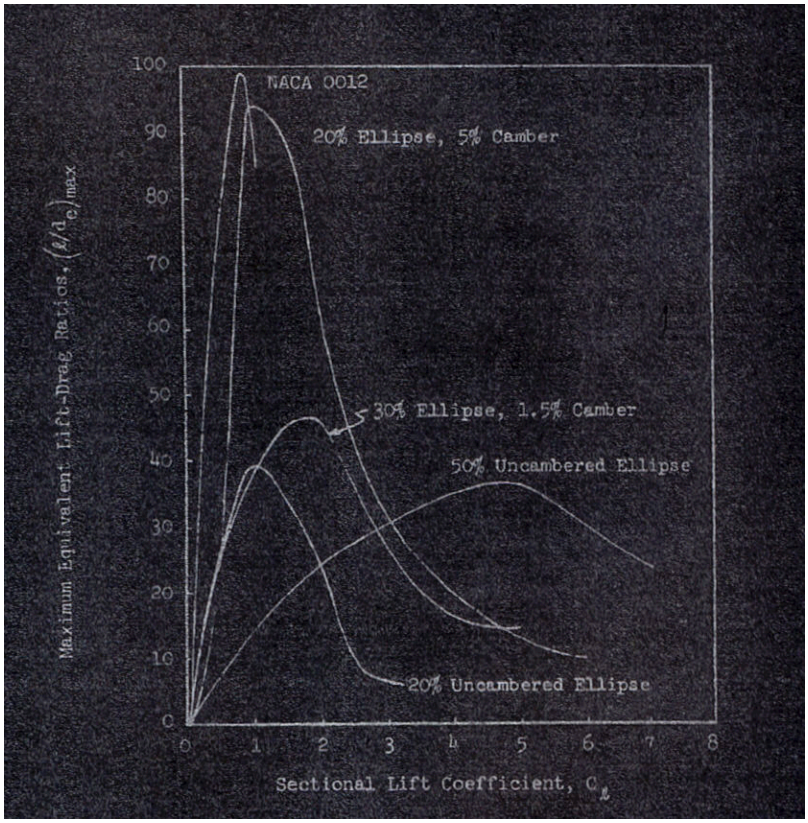

Figure 10.5. Experimental results - efficiency comparison of standard NACA 0012 against circulation control ellipses. (Englar, 1971).

Most AUVs designed for survey missions do not require fast manoeuvring capabilities (Subsea7, 2003). It was shown in chapter 7 that a maximum control surface angle of around 7 degrees or a typical lift coefficient of 0.39 is sufficient for Seahorse/Geosub sized AUV systems. If the circulation control duct system was implemented on the Seahorse AUV it would therefore result in an efficiency improvement of 9.5 % relative to the conventional control plane system (figure 10.2).

10.4 Power requirements

The lift/drag ratio comparison is useful as it compares the efficiency of the new active duct system against the conventional passive control plane system but it may also be misleading from a system point of view. To produce lift in a circulation control system, jet pump power is required. Treated independently from the

propulsion unit, a normal control plane can maintain a lift force without any power input whereas a circulation control duct will require constant jet pump power. Assuming two jet slot quadrants are used together and span a combined 180 degrees round the duct, the jet pump power required can be defined as,

$$\text{Power} = \frac{1}{2}\cdot\rho\cdot h\cdot\frac{\pi\cdot D}{2}\cdot V_{jet}^{3}$$

Applying this formula to the Seahorse AUV example results in the power requirements for the circulation control system (ignoring losses). Figure 10.6 shows the power requirements at a high and low vehicle speed.

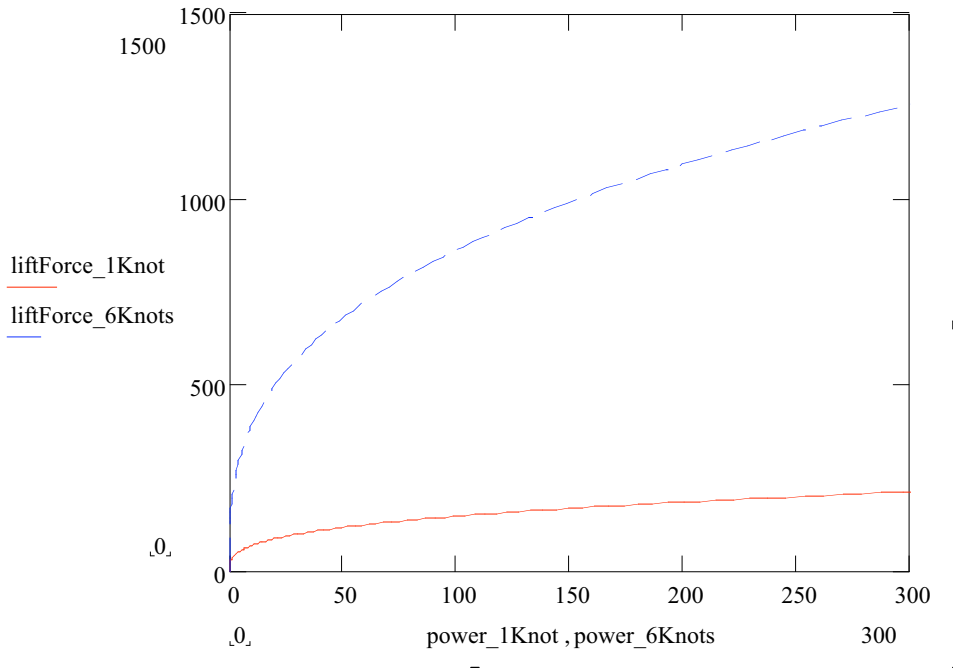

Figure 10.6. Power and lift force relationship.

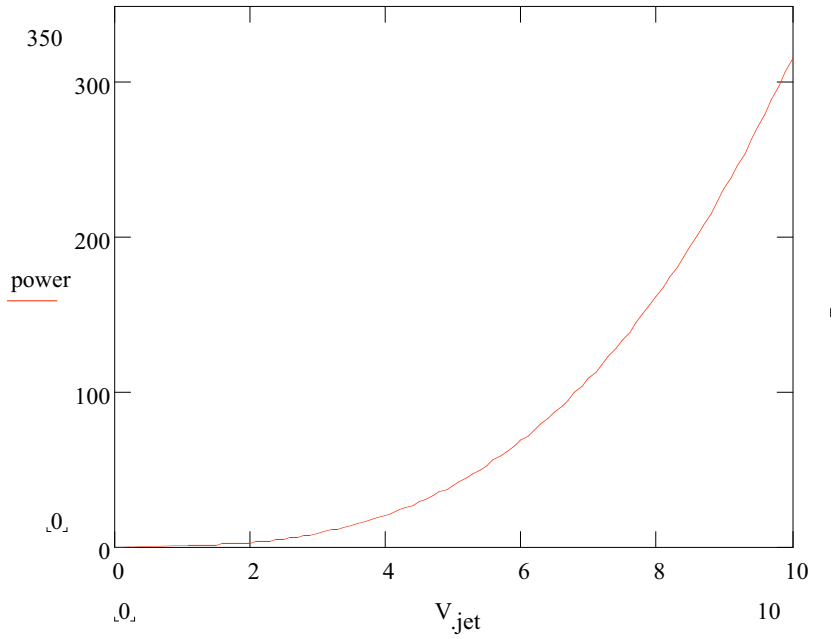

Figure 10.7. Power and jet velocity relationship.

To match the maximum manoeuvring force (700 N) of the Seahorse AUV with the new system, at a maximum vehicle speed of 6 Knots, a pump output power of 70 W is required.

Chapter 11. Discussion

The overall aim of the project was to show that the circulation control technique could be used on an AUV (that uses a ducted propeller) to generate a manoeuvring force at an efficiency that is at least equal to the traditional control surfaces. This was to allow the removal of the control surfaces. This has been proven to be possible with the new system having greater efficiency and superior manoeuvring force characteristics. These effects and practical matters are discussed in this chapter.

11.1 Manoeuvring force comparison

A major aim of the project was to compare the manoeuvring force produced by the circulation controlled duct system to the conventional AUV control plane system. In order to estimate the force produced by the modified duct it was necessary to develop a semi-empirical formula to calculate the induced lift force. This was described in chapter 5. The author is not aware of any other published formula similar to this that attempts to incorporate the effects of the trailing edge Coanda diameter and additional propeller thrust.

The model is based on a combination of other authors experiments and should only be regarded as an approximation. In particular, the effect of the Coanda diameter is only accurate for higher values of radius/chord ratios. It was also assumed in the model that the trailing edge was round. It is also possible to use an elliptical trailing edge successfully (Englar 1971) but this was not considered. The effect of Reynolds numbers is also an issue. Englar's tests on the super STOL aircraft model (upon which parts of the semi-empirical formula are based) were carried out at a Reynolds number of around $16x10^4$. The Reynolds number of the modified duct on the Seahorse AUV has a Reynolds number of a $12x10^4$ at 1 Knot and $73x10^4$ at 6 Knots. Therefore, the formula will have greater accuracy at lower speeds.

The induced lift force comparison was carried out assuming a large diameter trailing edge with a radius/chord ratio of 0.043. An original Marin 19a duct has a ratio of about 0.019. It is assumed that a ratio of 0.019 operates in the unpredictable zone (chapter 5) and that the lift force performance will be similar to a diameter of 0.043.

The magnitude of the manoeuvring lift force produced by the new system is dependent on the water jet velocity. In the force comparison (chapter 7), the velocity was adjusted so that the manoeuvring force was at least equal to the control plane system. Due to the different characteristics of the lift generation systems, this resulted in the force being matched at 6 Knots but produced a large improvement at lower speeds; 600 % improvement in lift at 1 Knot (figure 7.4). It is doubtful whether this improvement at lower speed is useful for current AUV operation since most modern survey AUVs will operate at a fixed speed. Low speed manoeuvrability is more of an issue on larger marine vehicles such as submarines and ships. Traditional ship rudders only work well at higher speeds. Analysis similar to the force comparison (chapter 7) was also done using a pelagic fishing trawler with a circulation control duct. At the trawler's maximum speed of 14 Knots, the manoeuvring force was shown to be equal to the trawler's single spade rudder but at 1 Knot showed a 1200 % improvement (Appendix B).

The effect of the duct's negative angle of attack on the circulation control system has been identified (chapter 5.6). This has the interesting characteristic of generating a forward thrust force component round the portion of the duct activated with circulation control. This effect has not been considered in other papers since circulation control is normally implemented on a wing with a positive angle of attack. Even with a submarine stern plane that can have a negative angle of attack (and uses circulation control), it is normally assumed that the trailing edge would have two jet slots (one at the top and one at the bottom). The jet blowing would only occur at one slot so that relative to the blowing slot, the angle of attack was always positive. Since this additional thrust force is a moment directed forward from one side of the duct, it is not thought that it would significantly improve the manoeuvring performance of the AUV.

11.2 Duct modifications

The identification of the geometric modifications required to be made to the original duct was a key aim of the project. The calculation of the induced lift force and efficiency were also reliant on this information being defined.

A modified duct section was presented in chapter 8. This revealed that a duct with a profile such as the common MARIN 19a requires relatively small changes to the profile shape. It was recommended that the trailing edge diameter of the original MARIN 19a duct should be increased in diameter slightly to ensure Coanda attachment of the blowing jet. It is also possible that the existing diameter is suitable but would require physical testing to confirm jet attachment and also that the lift coefficient curve was acceptable. More modern ducts may use a sharper trailing edge and this would require greater modification. This would involve replacing the sharp trailing edge with a round or elliptical edge and also modifying the leading edge to maintain the duct's original profile lift coefficient.

Four thin slots must be added round the trailing edge of the duct. Chapter 8 described a suitable slot height range but for the Seahorse AUV duct calculations this was set to 0.58 mm. This can be altered but will also alter the mass and velocity of water that must be supplied by the pump. Internally, arrangements are necessary to deliver the jet water to the slots. The detailed internal structure was not within the scope of this thesis.

This report has considered the circulation control technique based on a MARIN 19a duct profile. This profile shape is used on ships and marine vehicles that operate mostly in the ahead position. Ships that also require high performance astern manoeuvring normally use the MARIN 37 duct. The circulation control technique could be applied to this duct, but for astern operation, jet slots would also be required at the leading edge of the propeller duct. A control system would be required to switch over from trailing edge jets (for ahead operation) to leading edge jets (for astern operation).

11.3 Efficiency comparison

A major aim of the project was to compare the efficiency of the new circulation control duct system against the traditional AUV control plane system. This comparison was done in chapter 10 and showed that a maximum efficiency improvement of 9.5 % was possible for the Seahorse AUV example. It was assumed that like the Subsea7 Geosub AUV, the US navy Seahorse AUV only requires low values of lift coefficient (maximum of 0.4). The efficiency calculations assumed that the circulation control duct generated an identical manoeuvring force to the original control surfaces.

The fact that the theoretical efficiency of the new system is superior to the control plane system at lower lift coefficients is interesting. This is mainly due to the higher efficiency gained by transferring the lift force generation from a straight control surface to a duct. A duct is an annular surface and therefore has a higher effective aspect ratio and Oswald efficiency factor. These values are superior due to the absence of tip flow losses. In reality, the analysis has not considered the full system losses so a practical system will likely be less efficient when compared to the traditional control surfaces. Inefficiencies in a real system would include the water pump turbine, motor and lengths of pipe required to feed the duct. However, it is not though that the efficiency would be vastly lower than the traditional system.

In the calculation of the efficiency comparison, the induced lift force of the new system was calculated using the semi-empirical formula developed in chapter 5. The induced drag force was calculated using the semi-empirical formula developed in chapter 6. The profile drag was also required for the efficiency calculations and was discussed in chapter 9. However, the final efficiency calculation was based around the assumption that the duct was a modified MARIN 19a duct. This meant that the profile drag of the modified duct could remain the same as the original duct since the trailing edge was of a suitable diameter to allow jet attachment. In reality, a more modern duct may have a sharper trailing edge and as chapter 9 shows, the profile drag may increase tenfold when the duct is modified. This would reduce the overall efficiency gain of the new system.

Chapter 12. Conclusions

It has been proven theoretically that a modified propeller duct that implements the circulation control technique can be used successfully to generate a suitable manoeuvring force on an AUV. This would allow the control planes of an AUV to be removed.

The system would greatly reduce the number of mechanical parts associated with the manoeuvring system external to the AUV hull. This would be advantageous in terms of reducing the probability of external damage caused during launch and recovery. It would also result in reduced maintenance costs and reduced manufacturing costs due to an increase in the use of standard components.

In the U.S. Navy Seahorse AUV example studied in the report, the force performance was found to be capable of matching the conventional control planes at 6 Knots and improving it by 600 % at 1 Knot. Efficiency was improved by 9.5 %, however it is likely that this efficiency gain would not be realised in practise due to system losses. It was found that a MARIN 19a duct would require only a small increase in diameter to the trailing edge along with four thin slits and associated water jet delivery system. Other ducts with a sharper trailing edge would require more extensive modification to create a round or elliptical trailing edge and may also require modifications to the leading edge to maintain the section lift coefficient.

The circulation control duct is also suitable for use on other marine vehicles and is particularly attractive in its ability to improve low speed manoeuvrability. When applied to a pelagic fishing trawler that used a ducted propeller, a manoeuvring force improvement of 1200 % was found at 1 Knot.

Chapter 13. Future work

The results of this report only estimate the performance of a circulation control duct and are based on previous authors experimental work in the aeronautical and marine fields. Therefore, it is recommended that a scale prototype of the circulation control duct should be built and tested. The effect of the propeller thrust on the circulation control induced force and drag has been based on scale aircraft wind tunnel tests and a half duct. With a full duct, induced lift and drag performance may differ from the semi-empirical formulas developed in this report. It also needs to be confirmed that a modified MARIN 19a duct's trailing edge diameter is capable of Coanda attachment and the resultant induced lift force performance measured. It was assumed in this report that the modified MARIN 19a trailing edge diameter would result in jet attachment and also perform favourably in terms of lift performance but this requires experimental verification. The profile drag also needs to be measured experimentally especially if a non-MARIN 19a duct required modification to adopt the technique.

Propeller cavitation may be an issue and requires testing. Additionally, since the circulation control only acts on one side of the duct, this may cause the propeller to become unbalanced. This may result in vibration and premature stern tube wear may occur. The circulation control duct is also likely to generate extra noise and this should be investigated. The detailed internal structure was not within the scope of this thesis and future work should look at this. The effect of the harsh marine environment is an important issue since corrosion and marine growth will affect performance. The implications of damage to the duct should also be investigated, damage would result in the slit geometry changing and the jet velocity would be affected. It is not clear how catastrophic the failure situation would be.

Appendix A considers a number of improvements that could be used with a circulation control duct to increase the basic performance further.

An interesting practical consideration is caused by an AUV having a single propeller. With a twin screw marine vehicle on a straight course, the propeller forces are balanced. However, on a single screw vehicle there will be an unbalanced force that will cause an unwanted manoeuvring force (Lewis, 1989). To maintain a straight ahead course, a small counter manoeuvring force is normally generated using a small rudder angle. Similarly with a circulation controlled duct, this would mean that there would be a requirement for a small amount of force to be generated. This means that the pump system would always be activated to some extent to maintain an accurate course. This issue will reduce efficiency slightly and is worth consideration.

The system considered in this report would only be applicable on AUVs that use ducted propellers. Many AUVs do not use ducts and the control planes tend to be more vulnerable to damage (figure 1.2). A new invention is proposed that could apply the circulation control technique to a non-ducted propeller. The invention is a new type of propeller hub that utilises the circulation control technique and is shown in figure 13.1. A non-moving propeller hub system is used to provide the Coanda surface and the slot jets are fed by pipes that pass inside a hollow propeller shaft. A secondary shaft inside the outer shaft is also required to secure the end hub. It is unclear how well this device would perform since the slots are limited in size; however, they are situated in the centre of the complex flow which may be advantageous. The concept transmits the manoeuvring force through the stern tube

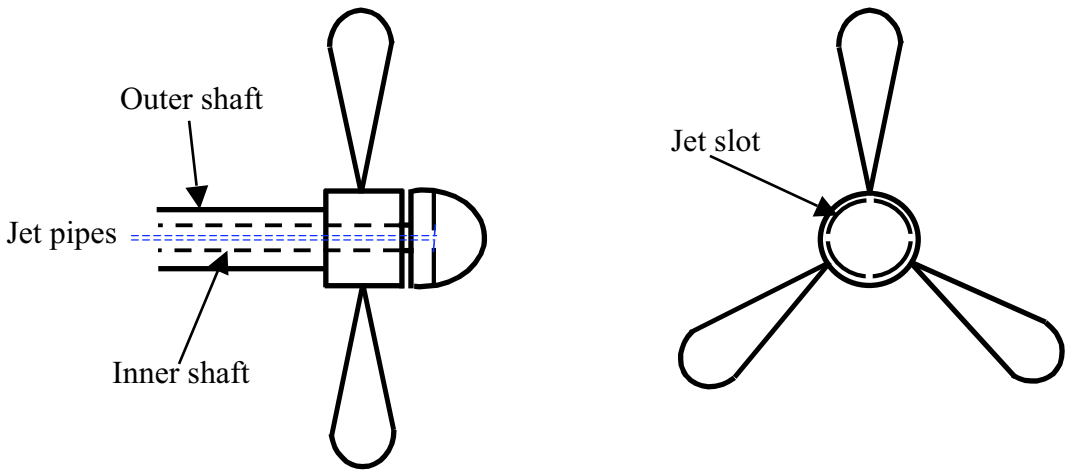

Figure 13.1. Proposed non-ducted propeller circulation control system.

so there may be an issue with stern tube wear. Cavitation is also an issue and there would be added complexity to the shafting system. This system would be particularly suited to AUV propeller systems since they tend to use large diameter hubs relative to the blade length. The concept would also have other applications in both nautical and aeronautical fields.

References

Ahn, H., Oh, J., K.H. (2000); “An experimental evaluation of the Coanda effect on a submerged flapped wing”, Proceedings of the 4th international conference on hydrodynamics, Yokohama, Japan. P133-138

Airforce-Technology, (2006); picture of Bell Boeing V-22 Osprey VTOL aircraft available from http://www.airforce-technology.com/projects/osprey/ last accessed 04.07.2006

Baker, W.J. and Paterson, E.G. (2004); “Rans and detached-eddy simulation of the NCCR airfoil”, Proceedings of the 2004 NASA/ONR Circulation Control Workshop, Hampton, March 2004, document NASA/CP-2005-213509/PT1, (p.167), available at http://hdl.handle.net/2002/15755 or http://library-dspace.larc.nasa.gov/, last accessed 18.05.2006

Bingham, D., Drake, T., Lott, R. (2002); “The application of autonomous underwater vehicle (AUV) technology in the oil industry – vision and experiences”, TS4.4 Hydrographic Surveying II, FIG XXII International congress, Washington D.C., April 19-26 2002. Available online at http://www.fig.net/pub/fig_2002/Ts4-4/TS4_4_bingham_etal.pdf, last accessed 26.08.2006

Breslin, J.P. and Andersen, P., (1994); ”Cambridge Ocean Technology, Series 3, Hydrodynamics of Ship Propellers”, Cambridge University Press, ISBN 0-521-41360-5

Bushnell, D.M. (1997); “Application frontiers of designer fluid mechanics-visions versus reality *or* *an attempt to answer the perennial question Why isn’t it used”* AIAA paper 1997-2110, June 1997

Cheeseman, I.C. and Seed, A.R., (1967); “The application of circulation control by blowing to helicopter rotors” Journal of the royal aeronautical society, Vol 71, July 1967, (451-467).

Clayton, B. and Bishop R.E.D (1982); “Mechanics of marine vehicles”, Gulf publishing company, ISBN 0-419-12110-2

Englar, R.J. and Williams, R.M. (1971); “Design of a circulation control stern plane for submarine application”, NSRDC report ASED-200, AD A 901-198, March 1971.

Englar R.J. (2004a); “Overview of circulation control pneumatic aerodynamics: blown force and moment augmentation as applied primarily to fixed-wing aircraft”, Proceedings of the 2004 NASA/ONR Circulation Control Workshop, Hampton, March 2004, document NASA/CP-2005-213509/PT1, p37-79, available at http://hdl.handle.net/2002/15755 or http://library-dspace.larc.nasa.gov/, last accessed 18/05/2006

Englar R.J. (2004b); “Experimental development and evaluation of pneumatic powered-lift super STOL aircraft”, Proceedings of the 2004 NASA/ONR Circulation Control Workshop, Hampton, March 2004, document NASA/CP-2005-213509/PT1, p101-121, available at http://hdl.handle.net/2002/15755 or http://library-dspace.larc.nasa.gov/, last accessed 18/05/2006

Englar, R.J. and Applegate, Constance A. (1983); “Circulation control – a bibliography of DTNSRDC rsearch and selected outside references”, David W. Taylor naval ship research and development centre Bethesda, Maryland, DTNSRDC-84/052, AD-A146 966, can be purchased from www.stormingmedia.co.uk.

English, J.W., (1967); “One-dimensional ducted propeller theory. Influence of tip clearance on performance”, National Physical Laboratory, U.K, ship division, Ship report 94, May 1967.

Griffiths, G., Fernandes P.G, Brierley A.S., Voulgaris G. (2001); ”Unescorted science missions with the autosub AUV in the North Sea”, International UUV Symposium, Newport, April 24-28, 2000, Available at http://www.soc.soton.ac.uk/OED/gxg/NUWC_unescorted_paper.pdf, last accessed 26.08.206

Howe, M.S. (2002); “Noise generated by a Coanda wall jet circulation control device”, Journal of sound and vibration, 2002, 249(4), p.679-700, available online at www.sciencedirect.com, last accessed 3.06.2006.

Javafoil (2006); airfoil analysis program, available online at http://www.mh-aerotools.de/airfoils/javafoil.htm last accessed 20.07.2006

Lewis, E.V., (1989); “Principles of naval architecture. Edition: 2nd revision” Society of Naval Architects and Marine Engineers, 1988-89, Vol. 2.

Loth (2004); ”Why have only two circulation controlled STOL aircraft been built and flown in years 1974-2004”. Proceedings of the 2004 NASA/ONR Circulation Control Workshop, Hampton, March 2004, document NASA/CP-2005-213509/PT2, p603, available at http://hdl.handle.net/2002/15755 or http://library-dspace.larc.nasa.gov/, last accessed 18.05.2006.

Lowry, J.G. and Vogler, R.D. (1956); “Wind-tunnel investigation at low speeds to determine the effect of aspect ratio and end plates on a rectangular wing with jet flaps deflected 85°”, NACA technical note, TN 3863, December 1956.

Mason, M.S. and Crowther, W.J. (2002); “Fluidic thrust vectoring of low observable aircraft” CEAS Aerospace Aerodynamic Research Conference, 10-12 June 2002, Cambridge, UK, available at http://www.geocities.com/m_mason007/home.html, last accessed 17.05.2006

MD Helicopters Inc. (2006); Manufacturer of NOTAR helicopter. Mesa, Arizona, USA. Website: www.mdhelicopters.com, last accessed 04.07.2006

Merry, S.L., Large M.J., Whitten T.J., Wilkinson M.R., Babb R.J (1996); "Control surface and actuator design for a low drag, laminar flow AUV", IEEE symposium on autonomous underwater vehicles 1996, Monterey, California, USA.

NAVOCEANO (1999); U.S. Naval Oceanographic Office, Stennis Space Center, U.S.A., https://www.navo.navy.mil/auv/auv_vehicles.html, last accessed 21.08.2006

Rhee, S.H., Kim, S.E. (2002); "Analysis of a jet-controlled high-lift hydrofoil with a flap", Journal of Ocean Engineering 30 (2003) 2117-2136. Available online www.sciencedirect.com last accessed 21.05.2006.

Rogers, E.O. and Donnelly, M.J. (2004); "Characteristics of a dual-slotted circulation control wing of low aspect ratio intended for naval hydrodynamic applications", AIAA 42nd Aerospace sciences meeting, Reno, NV Jan 2004, AIAA 2004-1244.

Subsea7 Ltd. (2003); Geosub AUV specifications, Subsea7 Ltd., Aberdeen, available at http://www.subsea7.com/rov_geosub.php, last accessed 23.08.2006.

Oosterveld, M.W.C, (1972); "Ducted propeller systems suitable for tugs and pushboats", International Shipbuilding Progress, Vol.19, No.219, 1972, p351.

Oosterveld, M.W.C. (1973); "Ducted Propeller Characteristics", Symposium on Ducted Propellers, Royal Institute of Naval Architects, London 1973, Paper No.4, p35.

Olds, Wm. Olds & Sons Pty. Ltd. (2006), Maryborough, Australia, Manufacturer of propeller ducts, company website http://www.olds.com.au/marine/, last accessed 3.07.2006.

ONR, (2006); U.S.Office of Naval Research, Arlington, Virginia. Website http://www.onr.navy.mil, last accessed 25.08.2006.

Weissinger, J. and Maass, D., (1968); ”Theory of the ducted propeller – a review”, 7th Symposium on naval Hydrodynamics, Office of Naval Research DR-148, pp 1209-1264.

Wood, N.J. and Nielsen, J.N., (1986); “Circulation control airfoils as applied to rotary-wing aircraft”, Journal of aircraft, published by AIAA, Vol. 23, No. 12, 1986, p865-875.

Zhu, S. and Wang, X. (1996); ”Experimental investigation of a high-lift rudder-circulation contol rudder”, International shipbuilding progress, 43(436):347-357, 1996.

Appendix A

Other performance enhancing improvements (at the expense of increasing complexity) could also be investigated. These include,

Harvell and Franke (1985) showed that extra secondary blowing further round the Coanda diameter edge can increase lift further.

Kondor and Moore (2004) used balanced circulation control round an entire duct's leading and trailing edges to create a "morphing" duct. The aim was to dynamically change the duct's basic profile lift and drag to improve the efficiency of a VTOL aircraft during both static (i.e. vertical take off) and cruise conditions. This effect could be useful for improving the efficiency of a marine ducted propeller during both bollard pull and ahead speed conditions. This may be useful for improving a duct's efficiency even if the circulation control was not used for generating a manoeuvring force.

Imber (2004) showed that alternating the blowing from a duct's slots resulted in counter-rotating vortices that produced a powerful braking effect. It is envisioned that this technique could be engaged far faster than it would take to reverse a standard propeller. This could be very useful in crash stop situations and for fast manoeuvring.

Appendix B

Mathcad Analysis of a Circulation Control Duct System / Traditional Rudder Force Comparison on a Pelagic Fishing Trawler

conversion definitions

$$deg := \frac{2\cdot\pi}{360} \qquad rpm := \frac{2\cdot\pi}{60} \qquad knots := 0.514$$

define main CC equations

$$funcC_T(n, D, V, K_T) := \frac{2\cdot n^2\cdot D^4}{V^2\cdot 191}\cdot K_T$$

$$F_L(C_L, \rho, A, V_{inf}) := C_L\cdot\frac{1}{2}\cdot\rho\cdot A\cdot V_{inf}^{\ 2}$$

$$F_D(C_D, \rho, A, V_{inf}) := C_D\cdot\frac{1}{2}\cdot\rho\cdot A\cdot V_{inf}^{\ 2}$$

$$C_\mu(h, c, V_j, V_{inf}) := 2\cdot\frac{h}{c}\cdot\left(\frac{V_j}{V_{inf}}\right)^2$$

$$AC_L(C_\mu, \phi, C_T, r, c, AOA) := \sqrt{C_\mu}\cdot\left(4\cdot\sin\left(\frac{\phi\cdot deg}{2}\right)\right)\cdot 0.83\cdot\left(\frac{C_T}{10}+1\right)\cdot\cos(AOA\cdot deg)$$

$$BC_L(C_\mu, \phi, C_T, r, c, AOA) := 1.4\cdot\sqrt{C_\mu} + 57.4\left(\frac{r}{c} - 0.0429\right) - 0.05$$

$$C_L(C_\mu, \phi, C_T, r, c, AOA) := AC_L(C_\mu, \phi, C_T, r, c, AOA) + BC_L(C_\mu, \phi, C_T, r, c, AOA)$$

$$C_D(C_L, AR, e, C_T, C_\mu) := \frac{C_L^{\ 2}}{\pi\cdot AR\cdot e} + 0.1\cdot\sqrt{C_\mu}\cdot C_T$$

Ship Velocity,	$startVelocity := 0.0514$ m/s $endVelocity := 7.2$ m/s (14 Knots) $velocityIncrement := 0.1$	
Duct Diameter	$D := 2.9$ m	
chord,	$c := 0.544D$ m	$c = 1.578$
slotheight,	$h := 0.002 \cdot c$ $\frac{m}{s}$	$h = 3.155 \times 10^{-3}$
coanda jet velocity,	$V_j := 65$	
coanda radius,	$r := 0.079$ m	
angle covered by slot,	$\phi := 180$ Degrees	
Propeller thrust coefficient,	$C_T := 0$	
Angle of attack,	$AOA := 0$	
Fluid Density,	$\rho := 1000$ $\frac{Kg}{m^3}$	
Aspect Ratio,	$AR := \frac{D}{c} \cdot 1.3$	$AR = 2.39$ (based on Imber, 2004)
Oswald efficiency factor,	$e := 1.17$	(1.17 for an annular wing, based on Imber, 2004)
Area of active portion of duct,	$A := c \cdot \pi \cdot D \cdot \frac{\phi}{360}$	

e.g. if 180 degrees of CC if used then A = 0.5 * total duct area

step up the freestream velocity

$increment := velocityIncrement \quad endvalue := endVelocity \quad startvalue := startVelocity$

$totalRange := endvalue - startvalue \qquad totalRange = 7.149$

$noSteps := \frac{totalRange}{increment} \qquad noSteps = 71.486$

$j := 1 .. (noSteps)$

$steppedValue_j := (j \cdot increment + startvalue)$

$V_{inf_j} := steppedValue_j$

$momentumCoefficient_j := C_\mu(h, c, V_j, V_{inf_j})$

$liftCoefficient_j := C_L(momentumCoefficient_j, \phi, C_T, r, c, AOA)$

$liftForce_j := F_L(liftCoefficient_j, \rho, A, V_{inf_j})$

$dragCoefficient_j := C_D(liftCoefficient_j, AR, e, C_T, momentumCoefficient_j)$

$dragForce_j := F_D(dragCoefficient_j, \rho, A, V_{inf_j})$

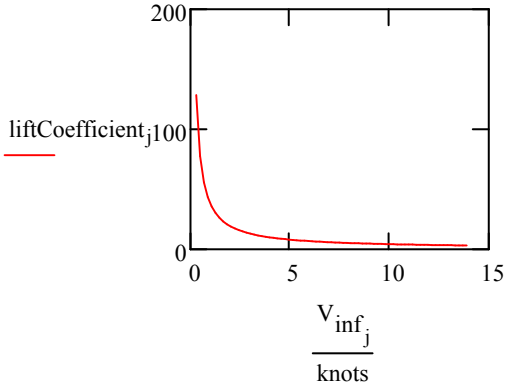

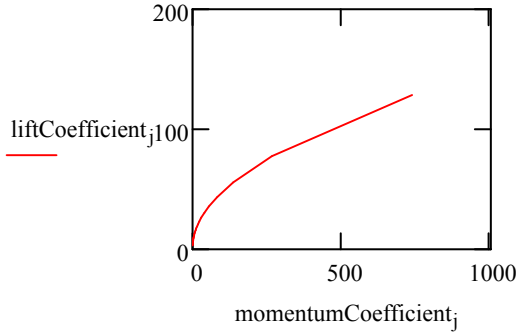

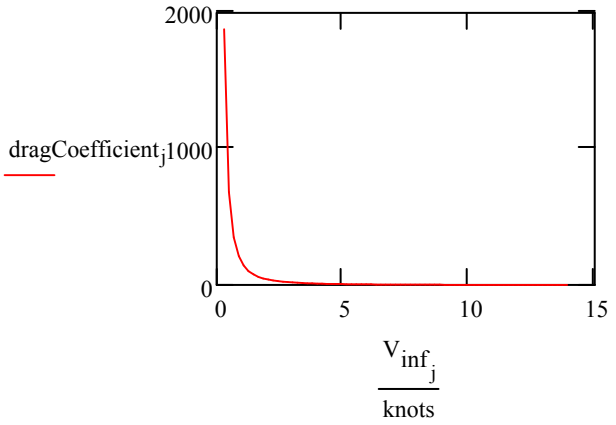

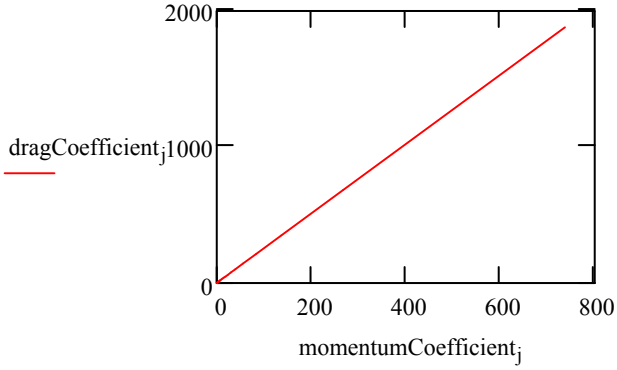

$C_T := 0.0$ $\quad liftCoefficientCt00_j := C_L(momentumCoefficient_j, \phi, C_T, r, c, AOA)$

$C_T := 0.5$ $\quad liftCoefficientCt05_j := C_L(momentumCoefficient_j, \phi, C_T, r, c, AOA)$

$C_T := 1.0$ $\quad liftCoefficientCt10_j := C_L(momentumCoefficient_j, \phi, C_T, r, c, AOA)$

$liftForceCt00_j := F_L(liftCoefficientCt00_j, \rho, A, V_{inf_j})$

$liftForceCt05_j := F_L(liftCoefficientCt05_j, \rho, A, V_{inf_j})$

$liftForceCt10_j := F_L(liftCoefficientCt10_j, \rho, A, V_{inf_j})$

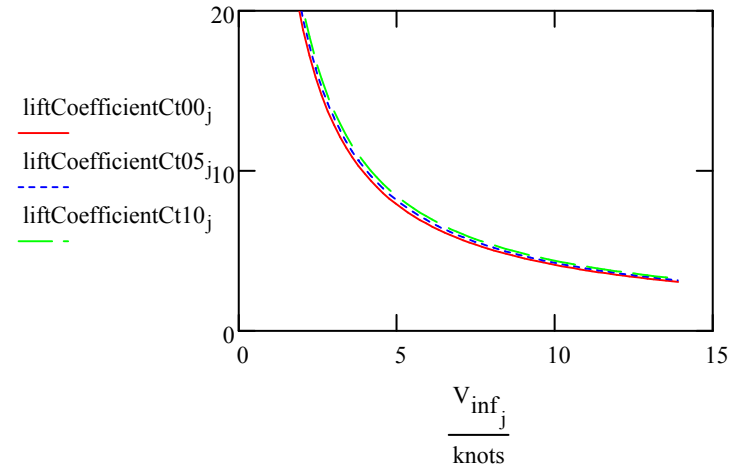

speed in Knots

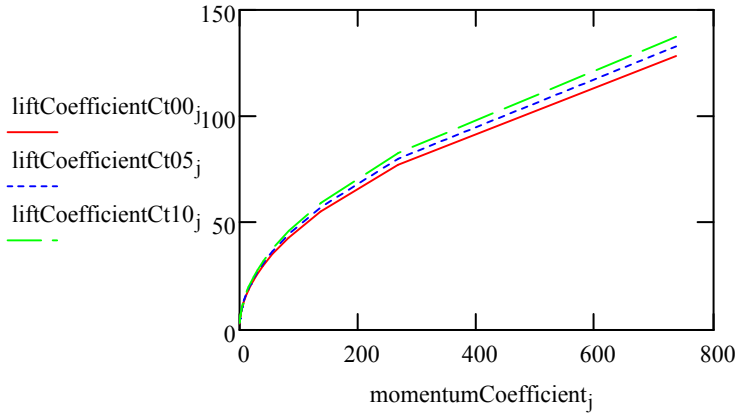

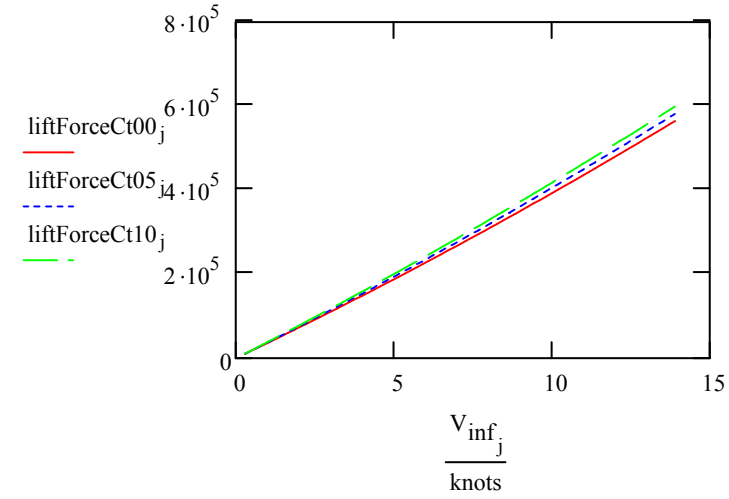

$C_T := 0.0$ $\quad dragCoefficientCt00_j := C_D\left(liftCoefficientCt00_j, AR, e, C_T, momentumCoefficient_j\right)$

$C_T := 0.5$ $\quad dragCoefficientCt05_j := C_D\left(liftCoefficientCt05_j, AR, e, C_T, momentumCoefficient_j\right)$

$C_T := 1.0$ $\quad dragCoefficientCt10_j := C_D\left(liftCoefficientCt10_j, AR, e, C_T, momentumCoefficient_j\right)$

$$dragForceCt00_j := F_L\left(dragCoefficientCt00_j, \rho, A, V_{inf_j}\right)$$
$$dragForceCt05_j := F_L\left(dragCoefficientCt05_j, \rho, A, V_{inf_j}\right)$$
$$dragForceCt10_j := F_L\left(dragCoefficientCt10_j, \rho, A, V_{inf_j}\right)$$

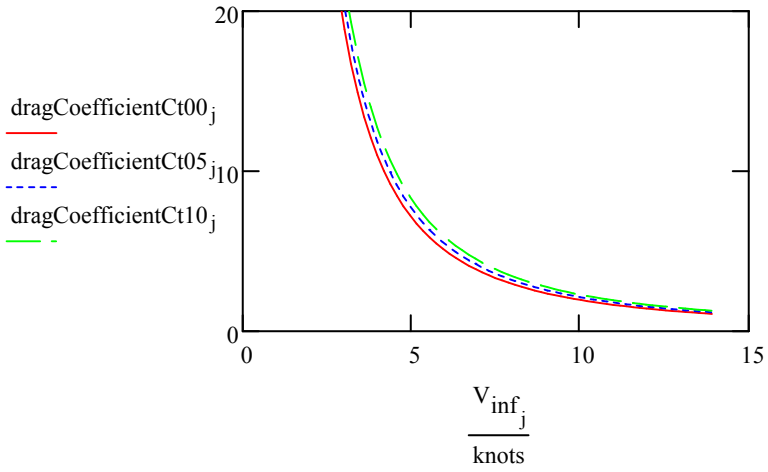

speed in Knots

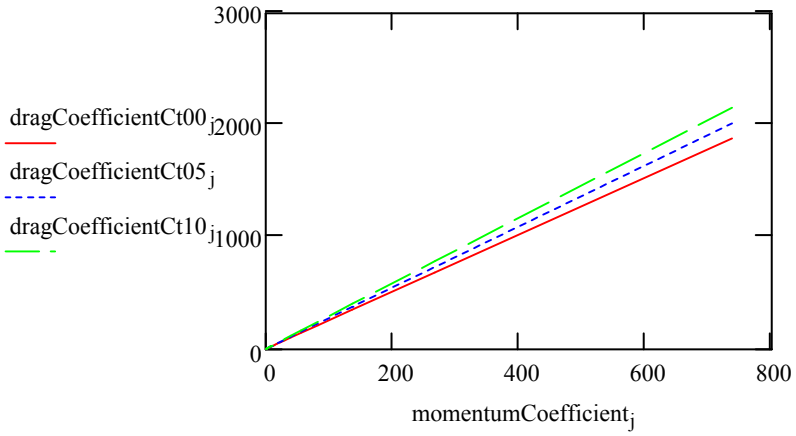

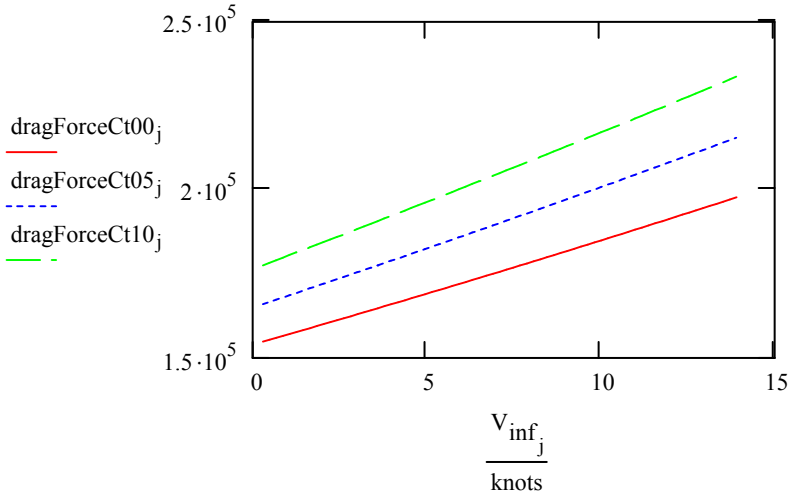

Effect of duct angle of attack

Decreasing the angle of attack to a negative value is necessary to develop the forward thrust of the duct that is fundamental to its operation. The negative angle of attack results in a horizontal component that is used to develop the forward thrust but the vertical component is cancelled out overall since the wing is circular. (However the duct must be strong enough to resist the vertical component forces)

It can therefore be seen that engaging circulation control blowing increases the lift over a section of the duct and this results in an unbalanced lift distribution that causes the desired manoeuvring force. If the angle of attack is zero then the induced lift force will be developed in the direction towards the centre axis of the duct. However if the angle is negative then is clear that the induced lift force will now have two components, one acting towards the centre of the duct and one acting forward.

AOAIncrement := 0.1

startAOA := −10

endAOA := 10

momentumCoefficient := 0.2

$C_T := 1.62$

$$\text{increment} := \text{AOAIncrement} \qquad \text{endvalue} := \text{endAOA} \qquad \text{startvalue} := \text{startAOA}$$

$$\text{totalRange} := \text{endvalue} - \text{startvalue} \qquad \text{totalRange} = 20$$

$$\text{noSteps} := \frac{\text{totalRange}}{\text{increment}} \qquad \text{noSteps} = 200$$

$$i := 1 .. (\text{noSteps})$$

$$\text{steppedValue}_i := (i \cdot \text{increment} + \text{startvalue})$$

$$\text{AOA}_i := \text{steppedValue}_i$$

$$\text{AngleofAttack} := 0 \qquad C_{\text{Loriginal}} := C_L(\text{momentumCoefficient}, \phi, C_T, r, c, \text{AngleofAttack})$$

$$C_{\text{Loriginal}} = 2.713$$

The extra forward thrust, $C_{\text{FTextra}_i} := C_{\text{Loriginal}} \cdot \sin(-1 \cdot \text{AOA}_i \cdot \text{deg})$

$$C_{\text{Dzeroangle}} := C_D(C_{\text{Loriginal}}, AR, e, C_T, \text{momentumCoefficient})$$

$$C_{\text{Langle}_i} := C_L(\text{momentumCoefficient}, \phi, C_T, r, c, \text{AOA}_i)$$

$$C_{\text{Dangle}_i} := C_D(C_{\text{Langle}_i}, AR, e, C_T, \text{momentumCoefficient})$$

The extra drag, $C_{\text{Dextra}} := C_{\text{Dangle}} - C_{\text{Dzeroangle}}$

Increase in forward thrust, $C_{\text{FT}_i} := C_{\text{FTextra}_i} - C_{\text{Dextra}_i}$

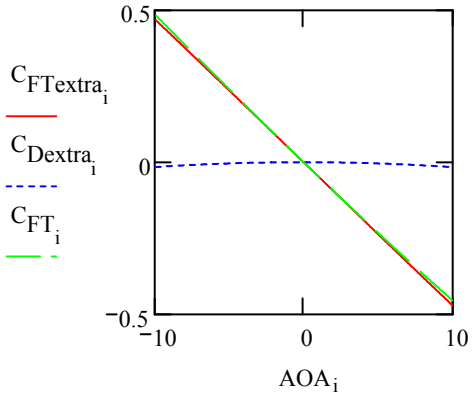

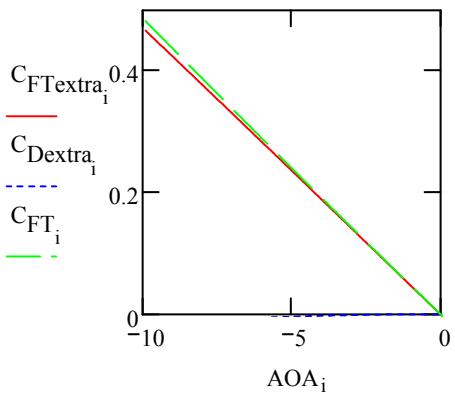

It can be seen that for a negative angle of attack, there is an overall gain in forward thrust during manoeuvring. As the angle of attack increases, the lift increases but as can be seen from the graph the drag hardly increases so this results in an overall gain in forward thrust. Although circulation control blowing is used here to generate the induced lift, the basic principles of increasing the angle of attack are the same as basic aerodynamics and the results are as expected.

$$\text{funcF}_{TFextra}\left(C_{TFextra}, \rho, V, A\right) := C_{TFextra} \cdot \frac{1}{2} \cdot \rho \cdot V^2 \cdot A$$

$C_{TFextra} := 0.775$ from the graph above at -10 degrees

$$A := c \cdot \frac{\pi \cdot D}{2}$$

$$F_{TFextra_j} := \text{funcF}_{TFextra}\left(C_{TFextra}, \rho, V_{inf_j}, A\right)$$

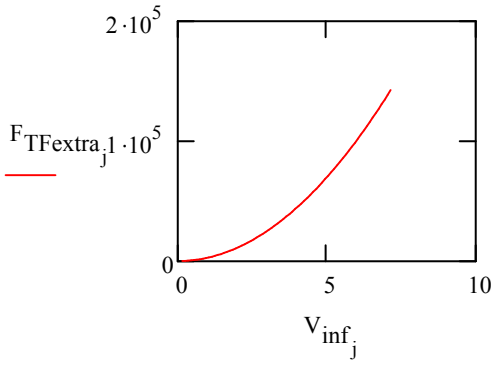

It can be seen that the induced forward thrust during manouvering increases as velocity increases. A normal rudder never produces a forward thrust since under deflection the resultant lift/drag force will be directed aft and port or starboard.

Thrust produced by the trawler with a traditional rudder is,

Propeller rpm $n := 180 \cdot rpm$

$K_T := 0.5$

$T_{orig} := \rho \cdot n^2 \cdot D^4 \cdot K_T$ $T_{orig} = 1.257 \times 10^7$

$$\%forceIncrease_j := \frac{F_{TFextra_j}}{T_{orig}} \cdot 100$$

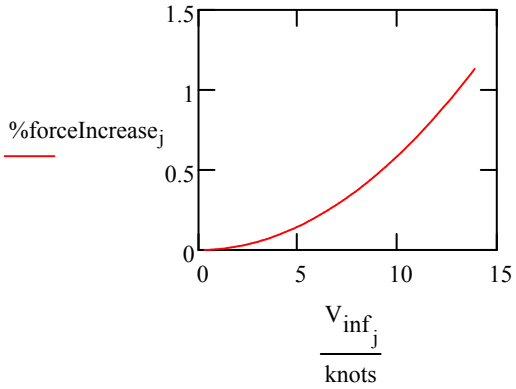

Analysis of a Traditional All-Movable Rudder

To compare the force it is necessary to use a rudder that would be typical for a ship.

Dummy value of Area,	$Area := 1$	
Angle of attack,	$\alpha := 10$	
Sweep angle of the quarter chord line,	$A := 11 \cdot deg$	
Oswald efficiency factor,	$e := 1.17$	
Minimun section drag coefficient,	$C_{do} := 0.0065$	0.0065 for NACA 0015
Profile drag,	$C_{do} := 0$	Set as zero as we are comparing Induced drag
Effective aspect ratio,	$a := 3$	
aspect Ratio,	$AR := \frac{a}{2}$	from Clayton and Bishop (1982)
Crossflow drag coefficient,	$C_{Dc} := 0.82$	some of these values are from principles of Naval Architecture book (Lewis, 1989)

main rudder equations

$$CL\alpha Ratio(a, A) := \frac{0.9 \cdot 2 \cdot \pi \cdot a}{57.3 \cdot \left(\cos(A) \cdot \sqrt{\frac{a^2}{\cos(A)^4}} + 4 + 1.8 \right)}$$

$$C_{Lrudder}(a, A, \alpha) := CL\alpha Ratio(a, A) \cdot \alpha + \frac{C_{Dc}}{a} \cdot \left(\frac{\alpha}{57.3} \right)^2$$

$$C_{Drudder}(C_{do}, C_L, AR, e) := C_{do} + \frac{C_L^2}{\pi \cdot AR \cdot e}$$

$rudderLiftCoefficient := C_{Lrudder}(a, A, 45)$ $\quad rudderLiftCoefficient = 2.621$

$$F_L(C_L, \rho, A, V_{inf}) := C_L \cdot \frac{1}{2} \cdot \rho \cdot Area \cdot V_{inf}^2$$

$$rudderLiftForce := F_L(rudderLiftCoefficient, \rho, Area, V_{inf})$$

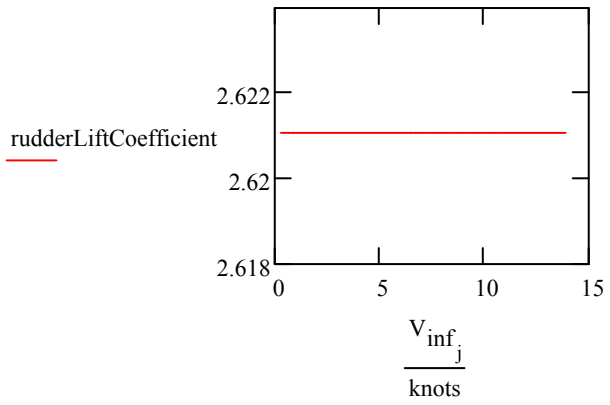

at alpha = 45

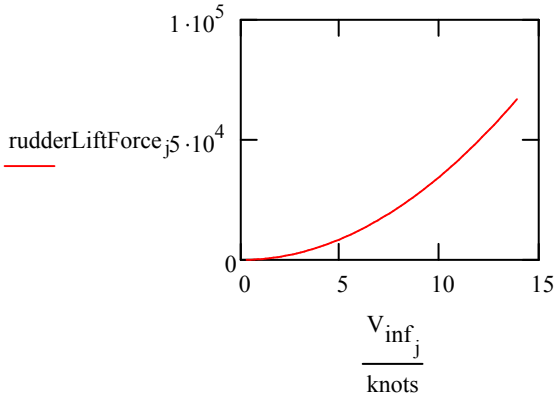

Effect of rudder angle

Keep the free stream velocity constant, $V_{inf} := 2$

$startAngle := 0$

$endAngle := 45$

$angleIncrement := 0.1$

$increment := angleIncrement \qquad endvalue := endAngle \qquad startvalue := startAngle$

$totalRange := endvalue - startvalue \qquad totalRange = 45$

$noSteps := \frac{totalRange}{increment} \qquad noSteps = 450$

$j := 1 .. (noSteps)$

$steppedValue_j := (j \cdot increment + startvalue)$

$\alpha_j := steppedValue_j$

$rudderLiftCoefficient_j := C_{Lrudder}(a, A, \alpha_j)$

$F_L(C_L, \rho, A, V_{inf}) := C_L \cdot \frac{1}{2} \cdot \rho \cdot A \cdot V_{inf}^{2}$

$rudderLiftForce_j := F_L(rudderLiftCoefficient_j, \rho, Area, V_{inf})$

$$\text{rudderDragCoefficient}_j := C_{Drudder}\left(C_{do}, \text{rudderLiftCoefficient}_j, AR, e\right)$$

$$F_D\left(C_D, \rho, A, V_{inf}\right) := C_D \cdot \frac{1}{2} \cdot \rho \cdot A \cdot V_{inf}^{\,2}$$

$$\text{rudderDragForce}_j := F_L\left(\text{rudderDragCoefficient}_j, \rho, \text{Area}, V_{inf}\right)$$

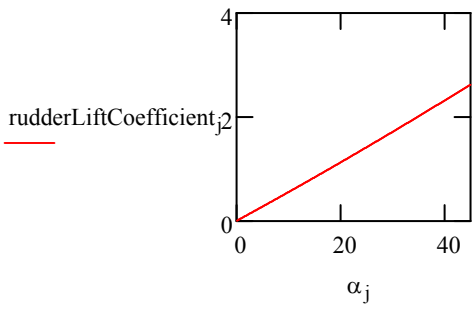

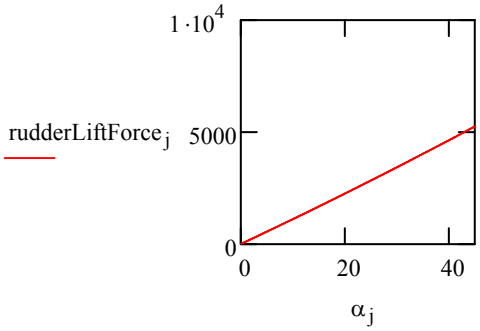

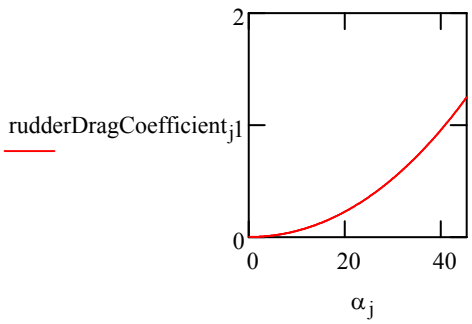

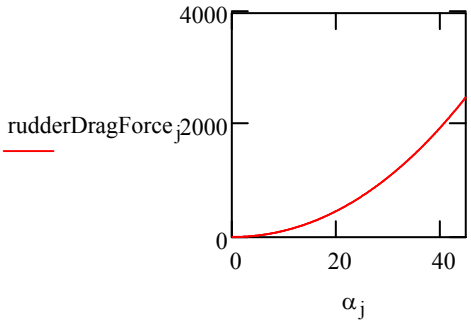

Trawler Comparison

It is necessary to use an example ship to make a good comparison since the size of the force produced is dependant on the size of the duct diameter. Take a Fishing Trawler such as the Danish built Menhaden, built in 1999. Details on specification sheet, available at Beara, www.beara.info/stories2004/menhaden_spec.htm, last accessed 26.08.2006.

Force produced by traditional rudder

A suitable rudder area can be defined by the DNV rule,

Draft,	$T := 4.8$	
Length,	$L := 41.3$	
Length between Perpendiculars,	$LBP := 0.95 \cdot 41.3$	Only the total length is given so estimate LBP.
Breadth,	$B := 10$	

$$rudderArea := \frac{T \cdot LBP}{100} \cdot \left[1 + 25 \cdot \left(\frac{B}{LBP} \right)^2 \right] \qquad rudderArea = 4.942$$

Since the actual kort nozzle for this ship is 2.9 m, an area of 5 m seems reasonable as this would mean the rudder dimensions were about 2.9 x 1.7m

The Induced force and drag can be calculated,

$$rudderLiftForce_j := F_L\left(rudderLiftCoefficient_j, \rho, rudderArea, V_{inf}\right)$$

$$rudderDragForce_j := F_L\left(rudderDragCoefficient_j, \rho, Area, V_{inf}\right)$$

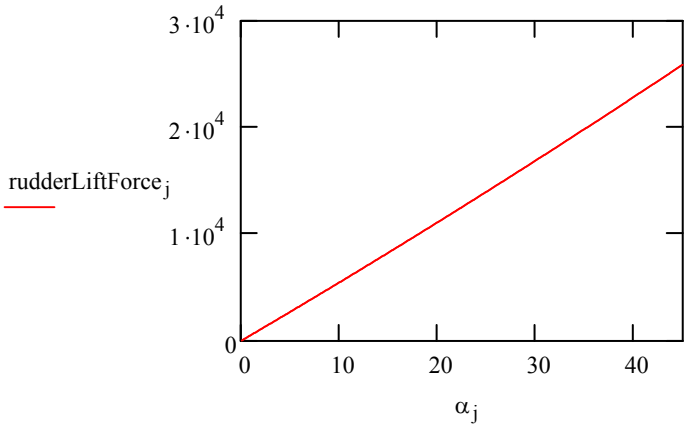

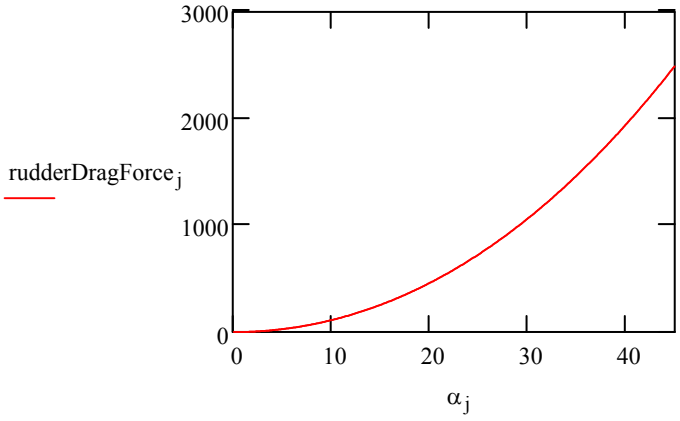

It is unclear when the rudder will actually stall but the trend and magnitude of the force produced is clear. A maximum angle of 45 degrees will be assumed.

$$startVelocity := 0$$

$$endVelocity := 10$$

$$increment := velocityIncrement \qquad endvalue := endVelocity \qquad startvalue := startVelocity$$

$$totalRange := endvalue - startvalue \qquad totalRange = 10$$

$$noSteps := \frac{totalRange}{increment} \qquad noSteps = 100$$

$$j := 1 .. (noSteps)$$

$$steppedValue_j := (j \cdot increment + startvalue)$$

$$V_{ship_j} := steppedValue_j$$

$$Knots_{ship_j} := \frac{V_{ship_j}}{0.514}$$

Maximum lift and drag forces (from graphs above), $C_{Lmax} := 2.62$ $C_{Dmax} := 1.27$

Therefore, assuming this maximum lift and maximum drag, the maximum rudder force can be calculated against velocity. Assume water velocity at rudder is 30% higher than the ship speed as suggested by Clayton and Bishop (1982)

$$V_{prop_j} := V_{ship_j} \cdot 1.3$$

$$rudderLiftForce_j := F_L\left(C_{Lmax}, \rho, rudderArea, V_{prop_j}\right)$$

$$rudderDragForce_j := F_L\left(C_{Dmax}, \rho, rudderArea, V_{prop_j}\right)$$

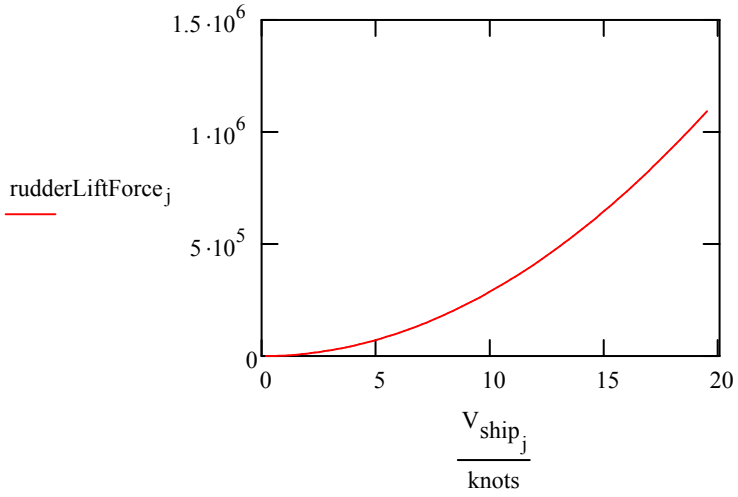

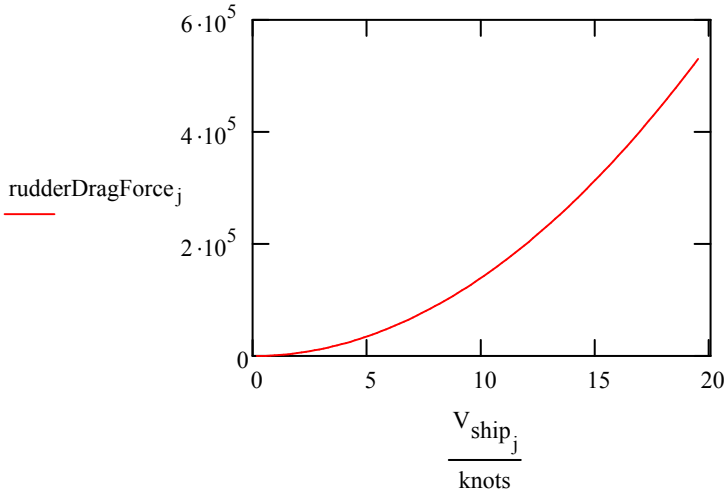

Force produced by circulation control duct

Now calculate the force produced by the CC duct system,

Duct Diameter	$D := 2.9$	m	
Chord,	$c := 0.544D$	m	$c = 1.578$
Slotheight,	$h := 0.002 \cdot c$	m	$h = 3.155 \times 10^{-3}$
Coanda jet velocity,	$V_{jet} := 60$	$\frac{m}{s}$	
Coanda radius,	$r := \frac{3.78 \cdot 10^{-2} \cdot 0.5 \cdot D}{2}$	m	$r = 0.027$ $r := 0.079$
Angle covered by slot,	$\phi := 180$	degrees	
Propeller Thrust Coefficient,	$K_T := 0.5$		
Propeller rpm	$n := 180 \cdot rpm$		
Ship speed @K.T below	$V := 14 \cdot knots \cdot 1.3$		
convert KT to CT	$C_T := funcC_T(n, D, V, K_T)$		$C_T = 1.503$
Angle of attack,	$AOA := -10$		for Marin 19A duct
Fluid Density,	$\rho := 1000$	$\frac{Kg}{m^3}$	
Aspect Ratio,	$AR := \frac{D}{c} \cdot 1.3$	$AR = 2.39$	(based on Imber 2004)

Oswald efficiency factor, $e := 1.17$ (1.17 for an annular wing, based on Imber, 2004)

$radius\_chord\_ratio := \frac{r}{c}$ $radius\_chord\_ratio = 0.05$ 0.02 <= r/c <=0.05

$slotHeight\_chord\_ratio := \frac{h}{c}$ $slotHeight\_chord\_ratio = 2 \times 10^{-3}$ 0.0005 <= h/c <=0.0025

Area of active portion of duct, $A := c \cdot \pi \cdot D \cdot \frac{\phi}{360}$

i.e. if 180 degrees of CC if used then A = 0.5 * total duct area

$momentumCoefficient_j := C_\mu(h, c, V_{jet}, V_{ship_j})$

$liftCoefficient_j := C_L(momentumCoefficient_j, \phi, C_T, r, c, AOA)$

$CCliftForce_j := F_L(liftCoefficient_j, \rho, A, V_{ship_j})$

$dragCoefficient_j := C_D(liftCoefficient_j, AR, e, C_T, momentumCoefficient_j)$

$CCdragForce_j := F_D(dragCoefficient_j, \rho, A, V_{ship_j})$

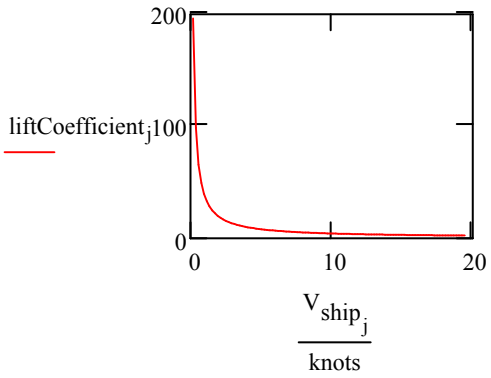

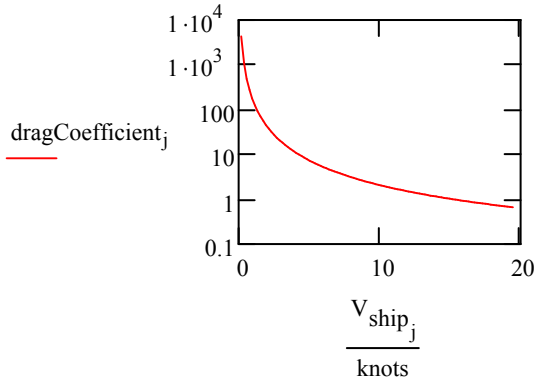

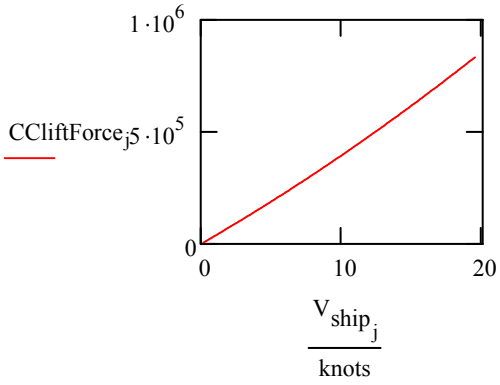

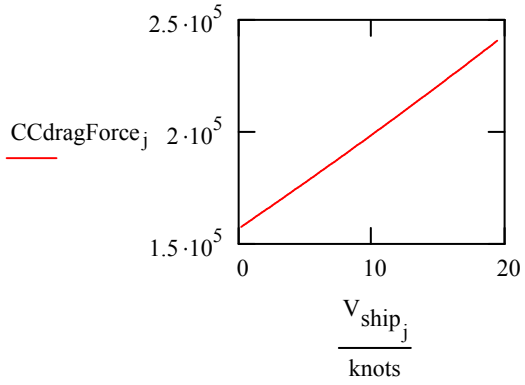

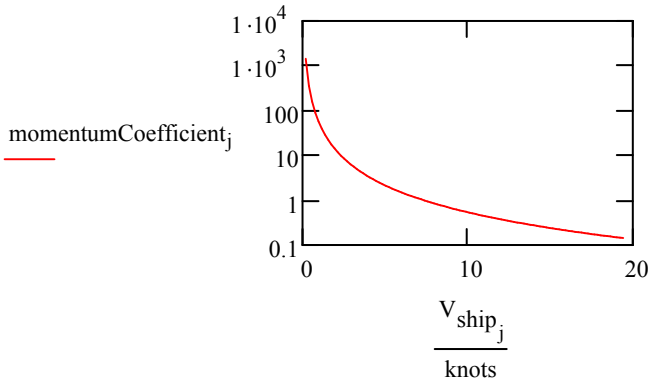

Comparison of traditional rudder and new CC system

Force comparison

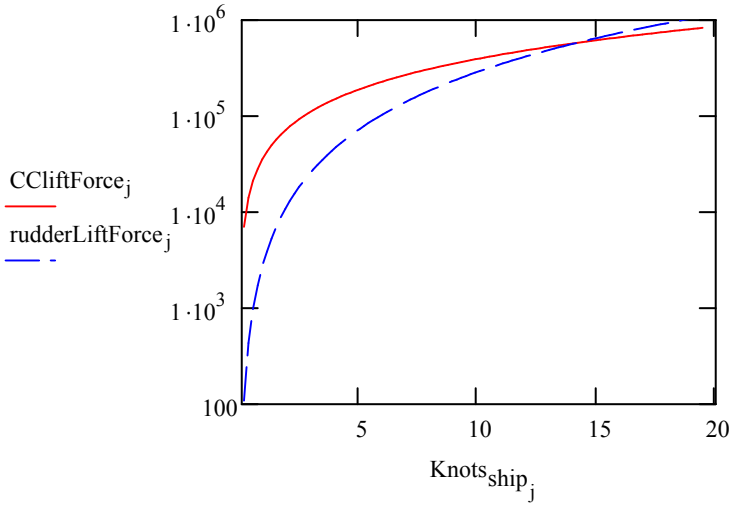

It can be seen from the graph above that there is a large difference in force produced by the CC system. The main advantage can be seen at lower speed as seen in the graph below.

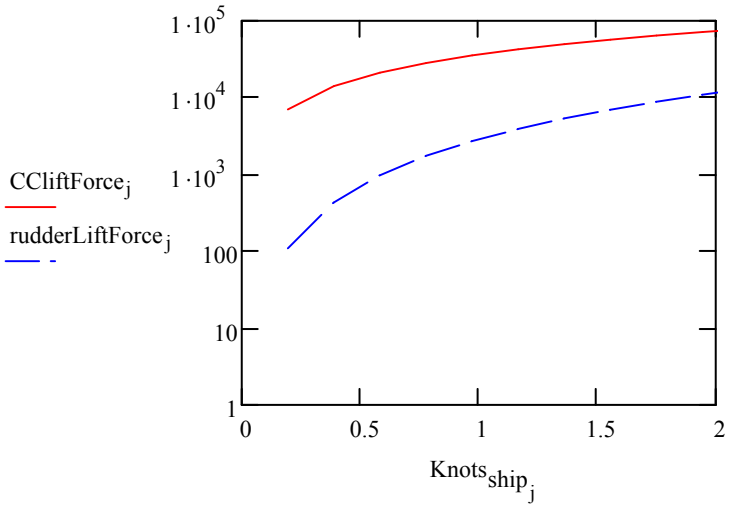

$$ForceImprovement\%_j := \frac{CCliftForce_j - rudderLiftForce_j}{rudderLiftForce_j} \cdot 100$$

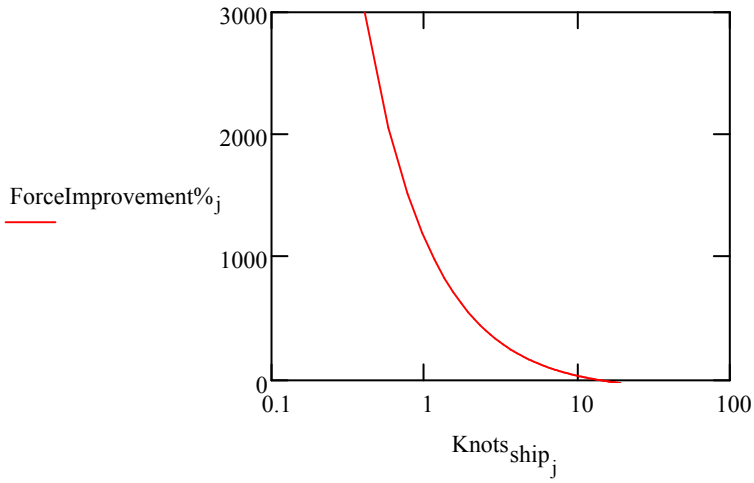

Induced drag comparison

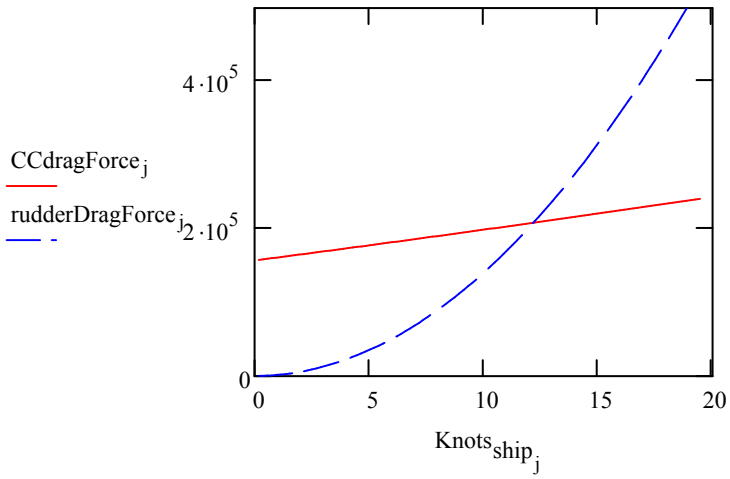

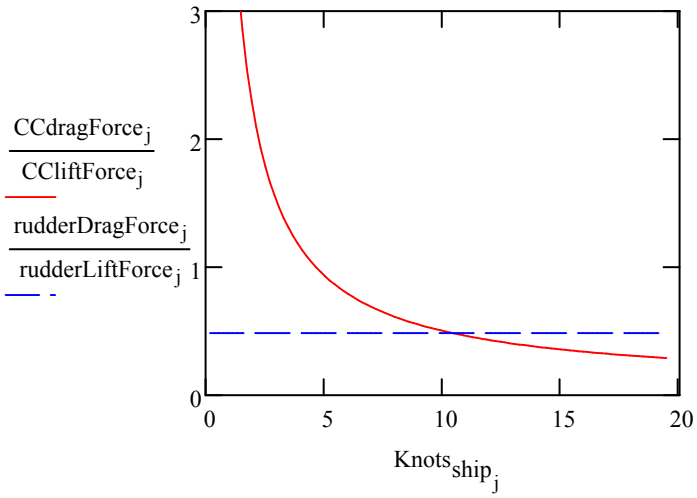

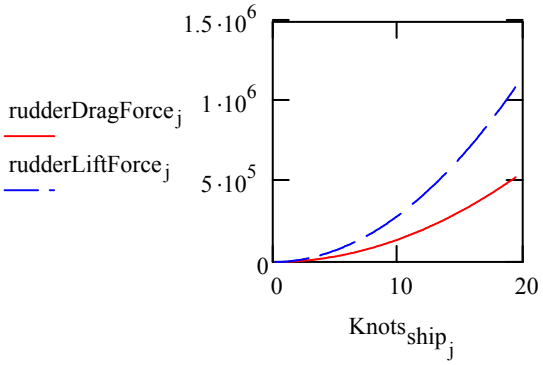

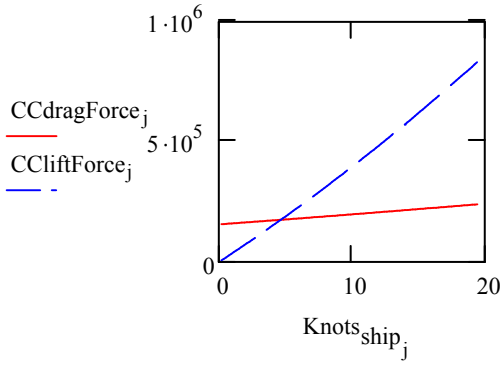

Extra forward thrust caused by negative AOA and CC induced lift

$$funcF_{TFextra}\left(C_{TFextra}, \rho, V, A\right) := C_{TFextra} \cdot \frac{1}{2} \cdot \rho \cdot V^2 \cdot A$$

$C_{TFextra} := 0.775$ from the previous analysis (above) at AOA = -10 degrees

Active area of duct, $Area := c \cdot \frac{\pi \cdot D}{2}$

Increase in forward thrust due to CC, $F_{TFextra_j} := funcF_{TFextra}\left(C_{TFextra}, \rho, V_{ship_j}, Area\right)$

Original propeller force, $T_{orig} := \rho \cdot n^2 \cdot D^4 \cdot K_T$ $T_{orig} = 1.257 \times 10^7$

$$\%forceIncreaseProp_j := \frac{F_{TFextra_j}}{T_{orig}} \cdot 100$$

$$\%forceIncreaseCC_j := \frac{F_{TFextra_j}}{CCliftForce_j} \cdot 100$$

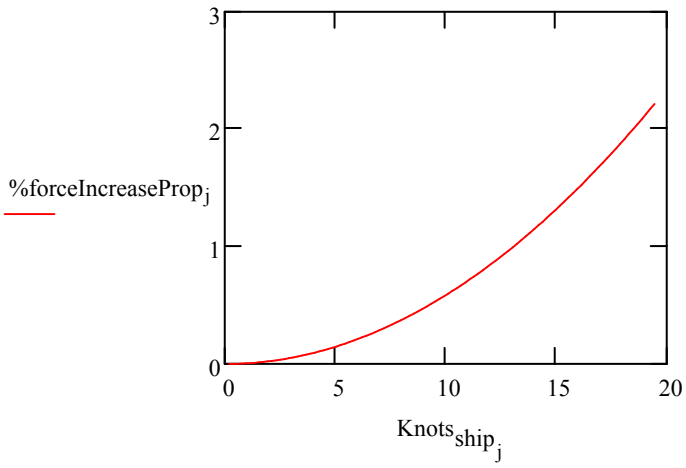
3
2
1
0
%forceIncreaseProp_j
0
5
10
15
20
Knots_ship_j

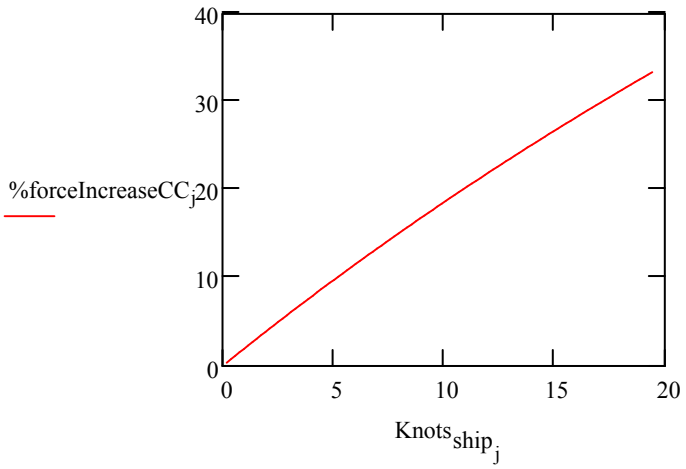
40
30
20
10
0
%forceIncreaseCC_j
0
5
10
15
20
Knots_ship_j